1987

Extending the Power Bandwidth of a Piezoelectric Bender Acutator

Jerrold Pavlinko
University of Central Florida

UNIVERSITY OF CENTRAL FLORIDA

OFFICE OF GRADUATE STUDIES

THESIS APPROVAL

DATE: April 6, 1987

I HEREBY RECOMMEND THAT THE THESIS PREPARED UNDER MY SUPERVISION

BY Jerrold Pavlinko

ENTITLED Extending The Power Bandwidth Of A Piezoelectric Bender Actuator

BE ACCEPTED IN PARTIAL FULFILLMENT OF THE REQUIREMENTS OF THE

DEGREE OF Master of Science in Engineering

FROM THE COLLEGE OF Engineering

Robert J. Martin
Supervisor of Thesis

RECOMMENDATION CONCURRED IN:

Robert L. Walker

Richard B. Miller

B E Mathews
Bruce E. Mathews
Coordinator of Degree Program

COMMITTEE ON FINAL EXAMINATION

L. M. Trefonas
Louis M. Trefonas
Dean of Graduate Studies

EXTENDING THE POWER BANDWIDTH OF A PIEZOELECTRIC BENDER ACTUATOR

BY

JERROLD PAVLINKO
B.S., Pennsylvania State University, 1978

THESIS

Submitted in partial fulfillment of the requirements
for the Master of Science in Engineering
in the Graduate Studies Program of the
College of Engineering
University of Central Florida
Orlando, Florida

Spring Term
1987

TABLE OF CONTENTS

LIST OF TABLES

LIST OF FIGURES

INTRODUCTION

Scanning mirrors are a control element used in electro-optical systems. A scanning mirror system is a position control system that directs an image to an optical receiver or projects the output of an optical source to a target. A scanning mirror, as part of an infrared image generation system, could be used to scan an array of infrared detectors with a television camera to produce a raster image. Conversely, a scanning mirror could be part of a laser engraving system where the mirror moves the laser beam across the surface of a material to engrave characters, logos, or drawings in the material.

Piezoelectric devices are electromechanical transducers in that they produce motion in response to an applied voltage. In a scanning mirror system, piezoelectric benders are used as the mechanism that moves the mirror. A "motor" of this sort that utilizes piezoelectric elements is called an actuator. This "motor" has no moving parts that are subject to wear due to friction and eliminates problems associated with the inertia of gears and shafts that are inherent in motor-driven position control systems. For these reasons, piezoelectric actuators are considered solid-state devices that produce motion.

This thesis examines an existing scanning mirror system that uses a piezoelectric actuator that was built by Thomas Tomasetti as part of the research for his master's thesis.[11] This system has performance limitations that restrict the power bandwidth of the system. The power bandwidth of a system is part of the large-signal response, and in this case, prevents the scanning mirror system from producing maximum mirror deflection at the high frequency end of its small-signal bandwidth. Due to the limited power bandwidth, the response time of the system is poor. The system also has a significant, although finite, position error that is over 9 percent. The purpose of this research is to present design modifications to the original scanning mirror system that improve the performance of the system and overcome some of the restrictions that are described above. Modifications are proposed that eliminate the steady-state position error and increase the power bandwidth.

This thesis begins with a brief description of the applications for ceramic piezoelectric devices, describes the manufacturing process, and explains the piezoelectric effect that is used by the scanning mirror system. This effect is then detailed as it applies specifically to the piezoelectric benders that are the main part of the actuator used by the system. An equivalent circuit model for the piezoelectric bender is presented that is used for all subsequent analysis.

Next, the implementation and performance of the original scanning mirror system is discussed and its limitations and

shortcomings are identified. A method of attenuating the resonances of the benders, using biquadratic notch filters, is presented. Other system performance considerations are discussed that point to the need for a series compensator. The lag-lead compensator design that encompasses these considerations is detailed in the section that follows. Finally, the performance of the modified system is examined to show the improvement in system performance.

CERAMIC PIEZOELECTRIC DEVICES

There is a wide range of common applications that use ceramic piezoelectric devices. Some of these applications are stereo phonograph cartridges, microphones, and headphones. Other more specialized applications include underwater sound transducers, hydrophones, accelerometers, and ultrasonic cleaners. Ceramic material is used to make piezoelectric devices because it can be easily molded in nearly any desired shape. Commercially available ceramic piezoelectric devices can be obtained in shapes such as discs, blocks, plates, bars, rings, and tubes.[7]

The term piezoelectric means "pressure electricity." As pressure is applied to a device made of piezoelectric material, electricity is produced. Conversely, an applied electric field will produce a deformation of the material. The amount of deformation that a piezoelectric device produces in response to an applied electric field depends upon the ceramic material that it is made from. Piezoelectric materials in common use are barium titanate, lead zirconate, and lead titanate. One ceramic that possesses high motion sensitivity is called PZT-5B, an obvious reference to its composition of lead, zirconium, and titanium. These ceramics do not naturally exhibit

piezoelectric properties. These properties are induced in the materials during the manufacturing process.[9]

The creation of a ceramic piezoelectric device begins by molding the ceramic material to the desired shape and allowing it to dry. The material is next heated to vitrify its surface and electrodes are applied to the molded device, either by electroplating, vacuum deposition, or conductive epoxy.[5] Finally, the material is heated to the Curie Point, the characteristic temperature of the ceramic above which it loses its piezoelectric properties.[9] While at this temperature, a high voltage direct current polarizing field is applied to the electrodes of the device. The molecules of the ceramic are somewhat free to move at this temperature, so that the unbalanced electrical dipoles can align in the direction of the applied field. After a time with the voltage applied, the device is cooled and the molecules are restrained in the orientation of the applied field.[5]

As a result of the polarization process, the piezoelectric device experiences a permanent increase in dimension between the electrodes and a permanent decrease in dimensions parallel to the electrodes. When a DC voltage is applied to the electrodes of the device with the same polarity as the original polarizing field, the device expands temporarily in the direction between the electrodes and contracts in the directions parallel to the electrodes. Conversely, the device will temporarily expand parallel to the electrodes and

contract in the direction between the electrodes when a voltage of opposite polarity is applied. When the voltage is removed from the device, it returns to its original size. It is this property that makes piezoelectric devices useful as electromechanical transducers.[9]

This expansion and contraction for a simple piezoelectric plate is shown in Figure 1. The device shown consists of a layer of piezoelectric ceramic between two electrodes. Figure 1a shows thickness expansion as a result of the applied electric field. This expansion is a direct result of the strain induced in the piezoelectric plate. In this case, the strain generated is parallel to the surface normal. Such a piezoelectric device is known as a pusher.[11] In Figure 1b, the applied electric field causes transverse expansion of the piezoelectric plate. A piezoelectric device that produces strain perpendicular to the surface normal, which produces transverse expansion, is known as a bender.[11] The amounts of the deformations shown in Figure 1 are very small and are on the order of microinches.[9] In practice, the piezoelectric plates shown in Figure 1 are bonded to a thin metal vane, usually brass. This configuration is called a monomorph since only one body of ceramic material is used.[5]

contract in the direction between the electrodes when a voltage of opposite polarity is applied. When the voltage is removed from the device, it returns to its original size. It is this property that makes piezoelectric devices useful as electromechanical transducers.[9]

This expansion and contraction for a simple piezoelectric plate is shown in Figure 1. The device shown consists of a layer of piezoelectric ceramic between two electrodes. Figure 1a shows thickness expansion as a result of the applied electric field. This expansion is a direct result of the strain induced in the piezoelectric plate. In this case, the strain generated is parallel to the surface normal. Such a piezoelectric device is known as a pusher.[11] In Figure 1b, the applied electric field causes transverse expansion of the piezoelectric plate. A piezoelectric device that produces strain perpendicular to the surface normal, which produces transverse expansion, is known as a bender.[11] The amounts of the deformations shown in Figure 1 are very small and are on the order of microinches.[9] In practice, the piezoelectric plates shown in Figure 1 are bonded to a thin metal vane, usually brass. This configuration is called a monomorph since only one body of ceramic material is used.[5]

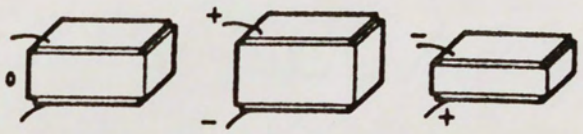

(a) Thickness Expansion.

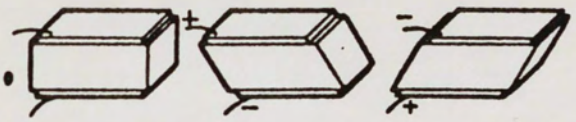

(b) Transverse Expansion.

Figure 1. Deformation of a Piezoelectric Plate.

PIEZOELECTRIC ACTUATORS

A monomorph in the form of a long cantilever-mounted bar that produces the transverse expansion shown in Figure 1b could be used in positioning applications. When mounted in this manner, the bar can be thought of as a series of incremental volumes of piezoelectric ceramic, placed side by side, that are polarized like that shown in Figure 1b. The incremental volumes are constrained at the bonded surface so that when a signal is applied, the sum of the incremental transverse expansions causes the bar to bend along its longitudinal axis.[3] Such an element is called a bender. The displacement of the free end of the bar from its neutral position can be orders of magnitude greater than that which can be obtained using a pusher.[11] Additional mechanical advantage can be gained to produce larger displacements of the free end of the bar by securing a second piezoelectric plate on the opposite side of the brass vane. The two plates are polarized in opposite directions so that an applied voltage causes the plates to deform in opposite directions. This configuration is called a bimorph because two bodies of ceramic material are used. "Bimorph" is a registered trademark of the Vernitron Piezoelectric Division and describes a flexure responsive piezoelectric device which has

the capacity to produce larger displacements than a monomorph.[9]

The piezoelectric benders used in the mirror scanning system developed by Tomasetti are bimorphs. They consist of two 0.009 inch thick layers of PZT-5B ceramic that are bonded to opposite sides of a 0.002 inch shim brass vane using epoxy. Fired on nickel electrodes cover the exposed surfaces of the ceramic.[10] Two 0.625 inch by 1.625 inch bimorph benders are cantilever-mounted as shown in Figure 2. The benders are polarized in the directions shown and the drive signal is applied to cause the benders to deflect in opposite directions. A small flat glass mirror, approximately three-quarters of an inch square and one-eighth of an inch thick, is mounted between the free ends of the two benders using double-sided adhesive foam tape as hinges. These hinges permit unrestricted motion of the benders without placing excessive stress on the mirror.[11] The linear displacement of the the free ends of the benders is transferred to produce an angular deflection of the mirror as shown in Figure 3.

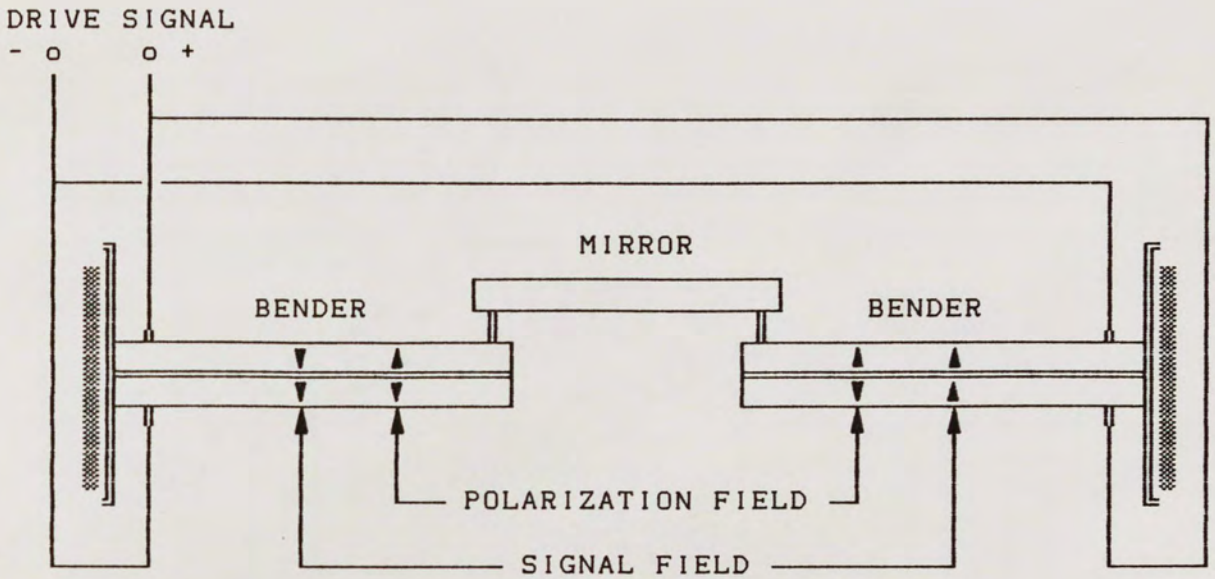

Figure 2. Cantilever-mounted Piezoelectric Bender Actuator.

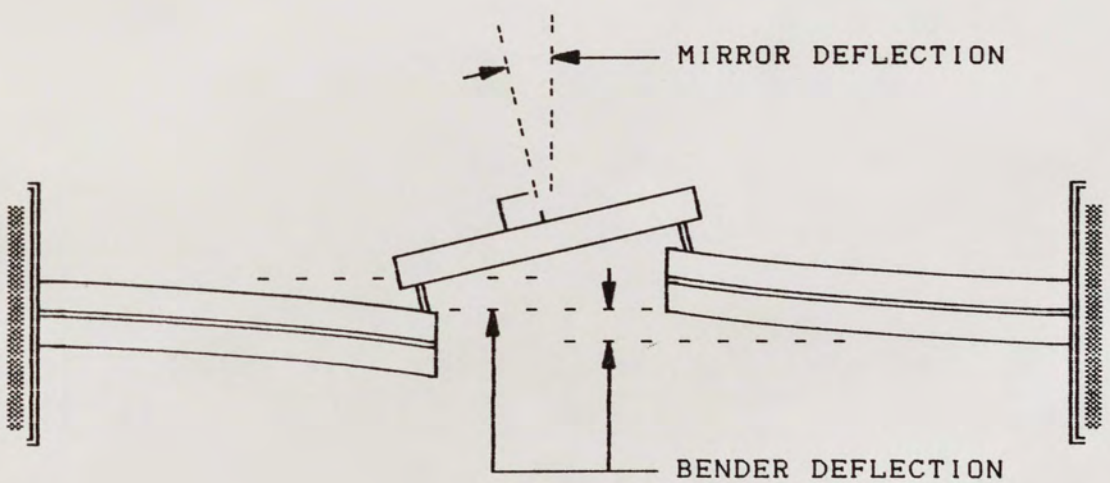

Figure 3. Actuator Deflection.

PIEZOELECTRIC BENDER MODEL

An equivalent circuit is used to describe the behavior of the piezoelectric elements used in the actuator shown in Figure 2. The circuit shown in Figure 4 relates the electrical behavior of the piezoelectric element to its mechanical behavior.[3] The inductor M' represents the effective vibrating mass of the element. The ideal transformer has no losses and no energy storage. The transformer ratio 1:N' has the units newtons/volt or coulombs/meter and relates input voltage to output force, input current to output velocity, or input charge to output displacement. The capacitor C_E' represents the electrical capacitance of the element while the capacitor C_M' represents mechanical compliance.[9] The equivalent circuit has the same resonant frequencies as the actual piezoelectric element. The heights of the resonant peaks of the bimorph are finite due to the inherent mechanical losses in the element. The values of the circuit elements in Figure 4 can be calculated using the electromechanical properties of the piezoelectric element and its physical dimensions.[3]

The circuit of Figure 4 can be transformed to a configuration more useful for designing a system to drive the actuator. The effective mass M' and mechanical compliance

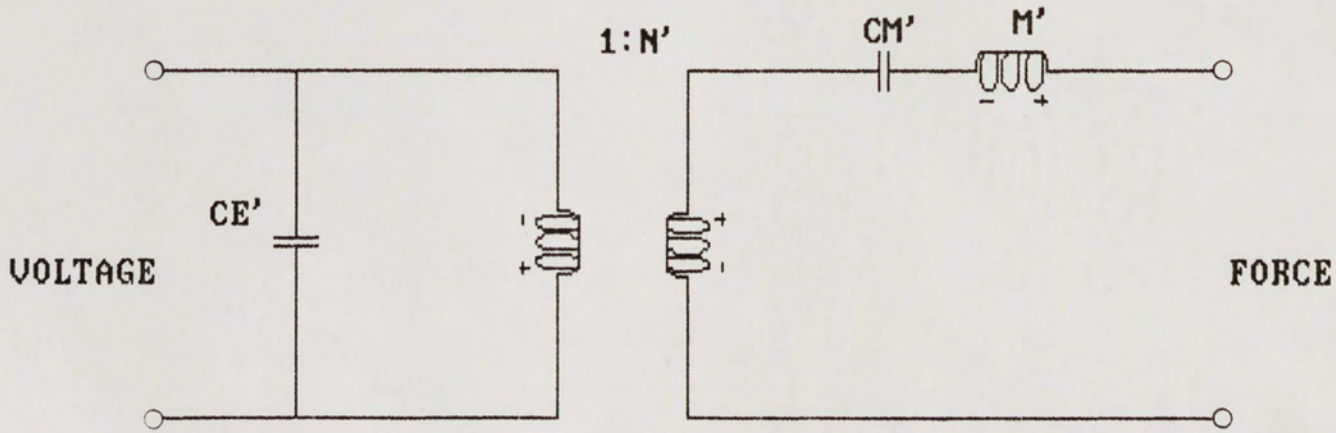

FIGURE 4. ELECTROMECHANICAL PIEZOELECTRIC MODEL.

C_M' can be translated to the input side of the ideal transformer. The dissipation of the piezoelectric element is taken into account by the addition of a series resistor. The resultant impedance model is shown in Figure 5 and consists of a capacitor C_E in parallel with a series RLC circuit. The capacitor C_E represents the electrical capacitance of the piezoelectric bender. The series RLC circuit represents the mechanical behavior and piezoelectric effect of the bender. The resistor R_M is the equivalent mechanical capacitance, the capacitor C_M is the equivalent mechanical capacitance, and the inductor L_M is the equivalent mechanical inductance. The inductor L_M is analogous to the mechanical mass while C_M represents the mechanical compliance. R_M represents the mechanical damping.

Tomasetti obtained values for the elements of the equivalent circuit model using an empirical method.[11] A plot of the input impedance of the piezoelectric bender is made using a spectrum analyzer. The resonant frequencies and the Q factor of the resonant peaks are determined from the plot. These values are used in an analytical expression for the input impedance of the piezoelectric bender to obtain the values of the circuit elements of the model.

An expression in the frequency domain for the input impedance of the model of Figure 5 is obtained using linear network analysis techniques and the voltage divider principle. The input impedance is

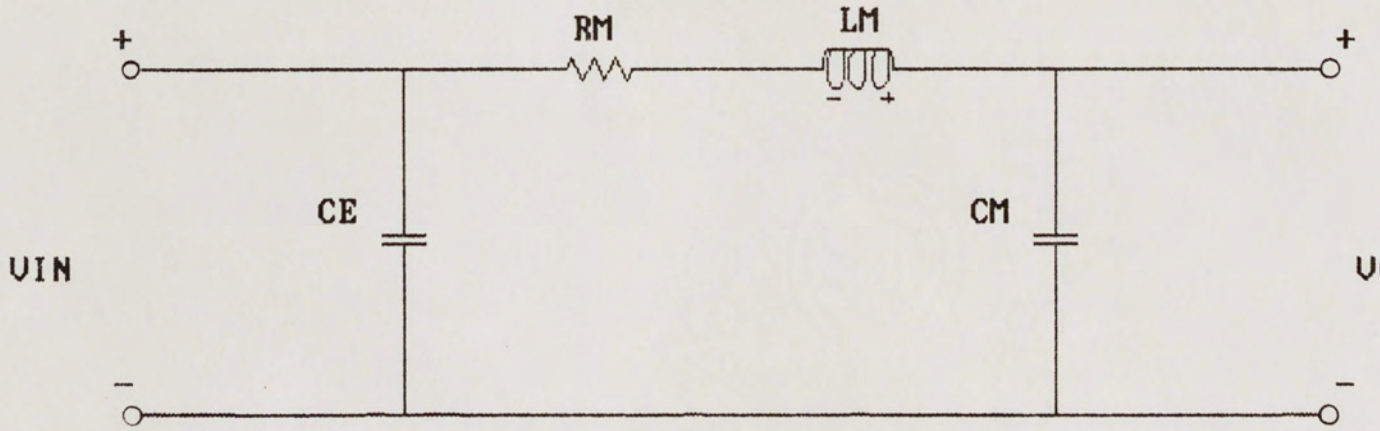

FIGURE 5. EQUIVALENT CIRCUIT PIEZOELECTRIC MODEL.

$$Z(s) = \frac{L_M C_M s^2 + R_M C_M s + 1}{(C_E + C_M)\, s \left[\dfrac{L_M C_E C_M s^2}{(C_E + C_M)} + \dfrac{R_M C_E C_M s}{(C_E + C_M)} + 1 \right]} .$$

This equation Z(s) above is of the same form as

$$Z(s) = \frac{\dfrac{s^2}{w_S^2} + \dfrac{s}{Q_S w_S} + 1}{C_T\, s \left[\dfrac{s^2}{w_P^2} + \dfrac{s}{Q_P w_P} + 1 \right]} ,$$

where w_S is the series resonant frequency, Q_S is the series quality factor, w_P is the parallel resonant frequency, Q_P is the parallel quality factor, and C_T is the total capacitance. Two equations for the series and parallel resonant frequencies are obtained by equating coefficients from the two preceding equations. The parallel resonant frequency w_P is

$$w_P^2 = \frac{C_E + C_M}{L_M C_E C_M}$$

and the series resonant frequency w_S is

$$w_S^2 = \frac{1}{L_M C_M} .$$

These two equations are combined to find C_M as

$$C_M = C_E \left[\frac{w_P^2}{w_S^2} - 1 \right] .$$

The electrical capacitance C_E is the input capacitance of the piezoelectric bender and is measured directly. The value for C_M is found using the above equation and this measured value. Once the value of the mechanical capacitance C_M is known, it is used in an expression for the mechanical inductance L_M that is obtained by solving the equation above for the series resonant frequency for L_M. This expression is

$$L_M = \frac{1}{w_s^2 C_M} .$$

Finally, the mechanical resistance R_M is found by equating the coefficients

$$\frac{R_M C_E C_M}{C_E + C_M} = \frac{1}{Q_s w_s} ,$$

which solved for R_M becomes

$$R_M = \frac{C_E + C_M}{Q_s w_s C_E C_M} .$$

The parameters obtained using the spectrum analyzer input impedance plot are

$$w_s = 1131 \text{ radians/second}$$

and

$$w_p = 1263 \text{ radians/second.}$$

The series quality factor Q_s is found using

$$Q_s = \frac{w_s}{B},$$

where B is the difference between the 3 dB frequencies on either side of w_s. The value of B is about 141 radians/second. This produces a value of Q_s equal to 8.0. The measured electrical capacitance C_E is 39.4 nF.[11]

The values of w_s, w_p, Q_s, and C_E are used in the above equations to find the values for R_M, L_M, and C_M. The values of the components of the equivalent circuit model are

$$R_M = 12694 \text{ ohms},$$

$$L_M = 80.4 \text{ henries},$$

and

$$C_M = 9.73 \text{ nanofarads}.$$

Figure 5 shows the equivalent circuit model for the piezoelectric bender with a single resonance at 180 Hz with the component values found using the empirical modeling technique.

The circuit elements in Figure 5 are lumped equivalents so that the circuit only approximates the actual behavior of the piezoelectric bender. This approximation is useful up to and slightly above the first resonant frequency. At higher frequencies, secondary resonances may occur due to the distributed nature of the mass and compliance.[9] A better approximation can be obtained by distributing the circuit

elements. A simple method of modeling a secondary resonance is to place a second series RLC circuit across the capacitor C_M in Figure 5. The model that results is shown in Figure 6. The values of the circuit elements that comprise the first RLC circuit are selected to produce the primary resonance while the values of the elements for the second RLC circuit are selected to produce the secondary resonance. As long as the values R_H and L_H in the second RLC circuit are selected to be much larger than R_M and L_M, the loading effect of the second RLC circuit on the first will be negligible.

The piezoelectric benders were found to have a secondary resonance about 1000 Hz. The magnitude of the resonant peak exhibits a Q of about 20.[11] With this information, an adequate set of values for the second RLC circuit in Figure 6 can be found. The value of C_H is arbitrarily selected as about one one-hundredth of C_M to produce values of R_H and L_H that are much larger than R_M and L_M. Passive filter design equations are used to find the values of the second RLC circuit.[12] The resonant frequency of a series RLC circuit is

$$w_o = \left[\frac{1}{L_H C_H} \right]^{1/2}$$

and the quality factor Q_o is

$$Q_o = \frac{w_o L_H}{R_H} = \frac{1}{R_H} \left[\frac{L_H}{C_H} \right]^{1/2} .$$

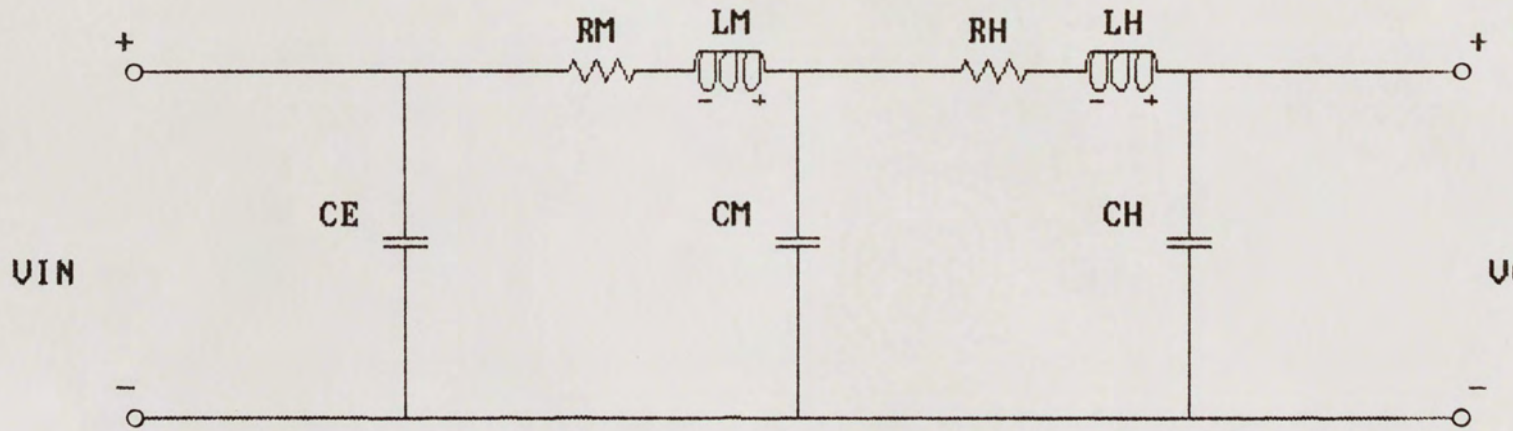

FIGURE 6. BENDER EQUIVALENT CIRCUIT MODEL.

These equations produce the component values

$$L_H = 281.46 \text{ henries}$$

and

$$R_H = 88442 \text{ ohms},$$

which, together with the value selected for C_H, implement a series RLC circuit with a resonant frequency w_o at 6283 radians/second and a quality factor Q_o of 20.

The model of Figure 6 is simulated using the Electronic Circuit Analysis Program MICRO-CAPII to produce the magnitude and phase response shown in Figure 7.[6] This plot shows the primary resonance at about 180 Hz and the secondary resonance at 1000 Hz accompanied by abrupt 180 degree phase changes at these frequencies.

The system transfer function $H_A(s)$ of the actuator model shown in Figure 7 has the form

$$H_A(s) = \frac{K_e}{\left[\frac{s^2}{w_{A1}^2} + \frac{s}{Q_{A1} w_{A1}} + 1\right]\left[\frac{s^2}{w_{A2}^2} + \frac{s}{Q_{A2} w_{A2}} + 1\right]},$$

where K_e is the electromechanical scale factor of the actuator. The value for K_e is found by driving the actuator with a known frequency and amplitude input signal while reflecting a laser source off the mirror attached to the actuator. The target is located a known distance from the mirror and the mirror is positioned to cause equidistant

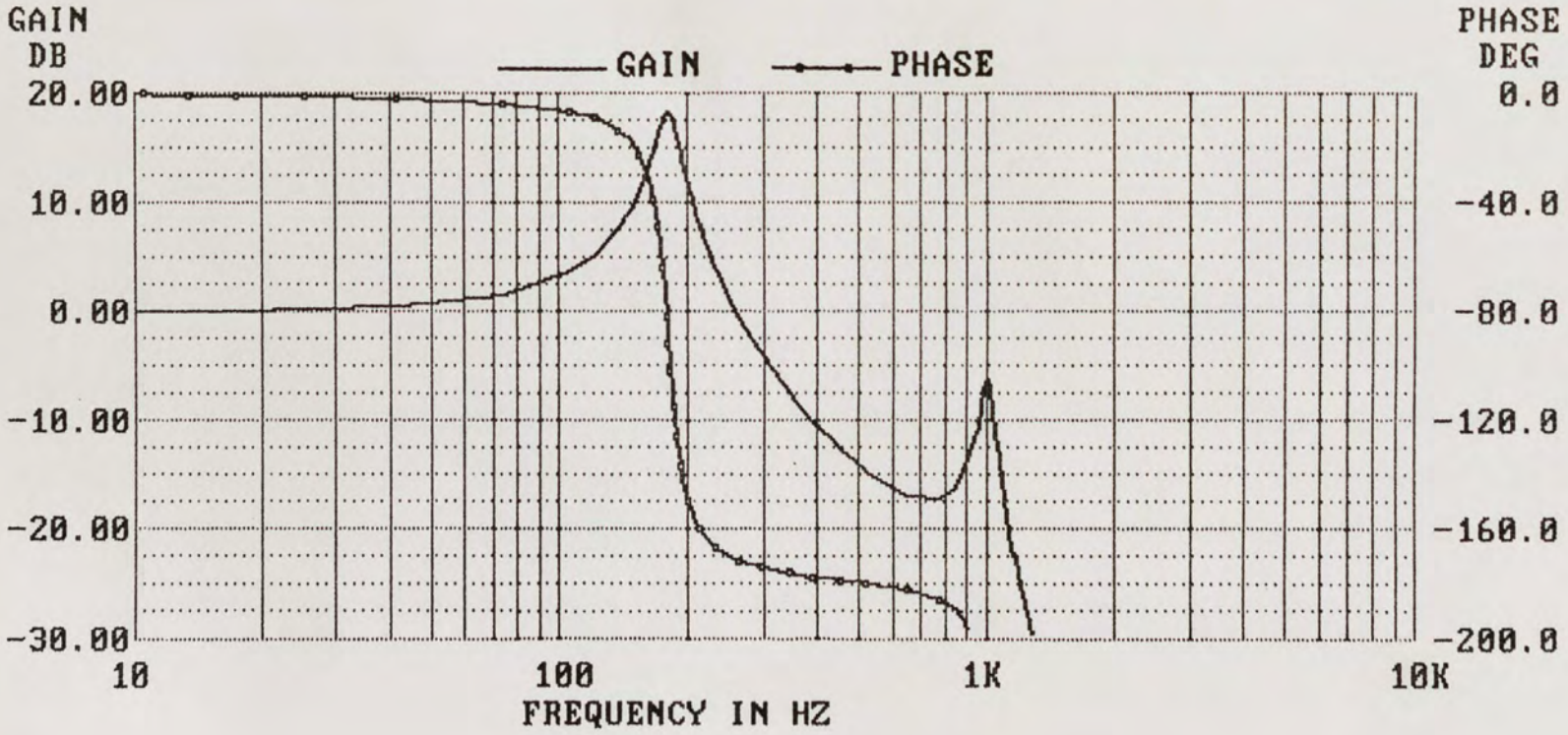

FIGURE 7. BENDER MODEL FREQUENCY RESPONSE.

deflections of the reflected light beam on either side of the target normal. The length of the line swept by the reflected light beam on the target is measured and trigonometry is used to determine the angular deflection of the beam. The actuator is driven with a 170 volt peak to peak signal at 60 Hz. The mirror is 113 inches from the target and the length of the line on the target is 11.5 inches. The angular deflection of the light beam is then 5.8 degrees per 170 volt swing. This translates to an electromechanical scale factor for the actuator model of

$$K_\theta = 598 \text{ microradians/volt.}$$

This completes the transfer function of the actuator model, which is rewritten as

$$H_A(s) = \frac{598 \times 10^{-6}}{\left[\frac{s^2}{(1131)^2} + \frac{2(.070)}{1131}s + 1\right]\left[\frac{s^2}{(6283)^2} + \frac{2(.025)}{6283}s + 1\right]}.$$

The actuator model of Figure 6 and its transfer function $H_A(s)$ are used for all subsequent system design.

SCANNING MIRROR SYSTEM

The system block diagram of the scanning mirror system developed by Tomasetti is shown in Figure 8. The actuator used by the system consists of a pair of cantilever-mounted piezoelectric benders described earlier and shown in Figure 2. Other system components shown are the position feedback, rate feedback, compensator, and power amplifier. Position feedback is obtained using a unique eddy current proximity detector and is used to extend the system bandwidth and eliminate the hysteresis that is characteristic of the piezoelectric benders. Rate feedback is derived from the current driving the actuator and is used to damp the primary resonance of the piezoelectric benders. The compensator is used to attenuate the secondary resonance of the actuator. The power amplifier is needed to produce voltages sufficient to drive the actuator. The system representation of the mirror scanning system is shown in Figure 9. The derivation of the transfer functions of each of the blocks shown is presented by Tomasetti.[11]

A schematic of the scanning mirror system control function is shown in Figure 10. This circuit realizes the blocks shown as A_{OL} and $H_c(s)$ in Figure 8. The inputs of this control circuit are the position feedback signal and the

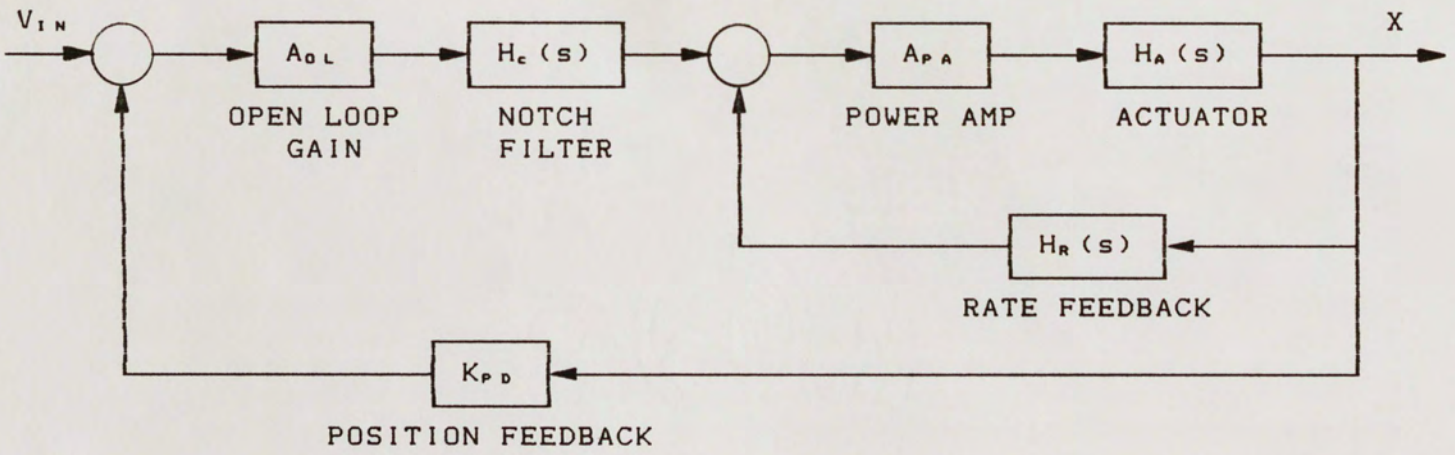

Figure 8. Scanning Mirror System Block Diagram.

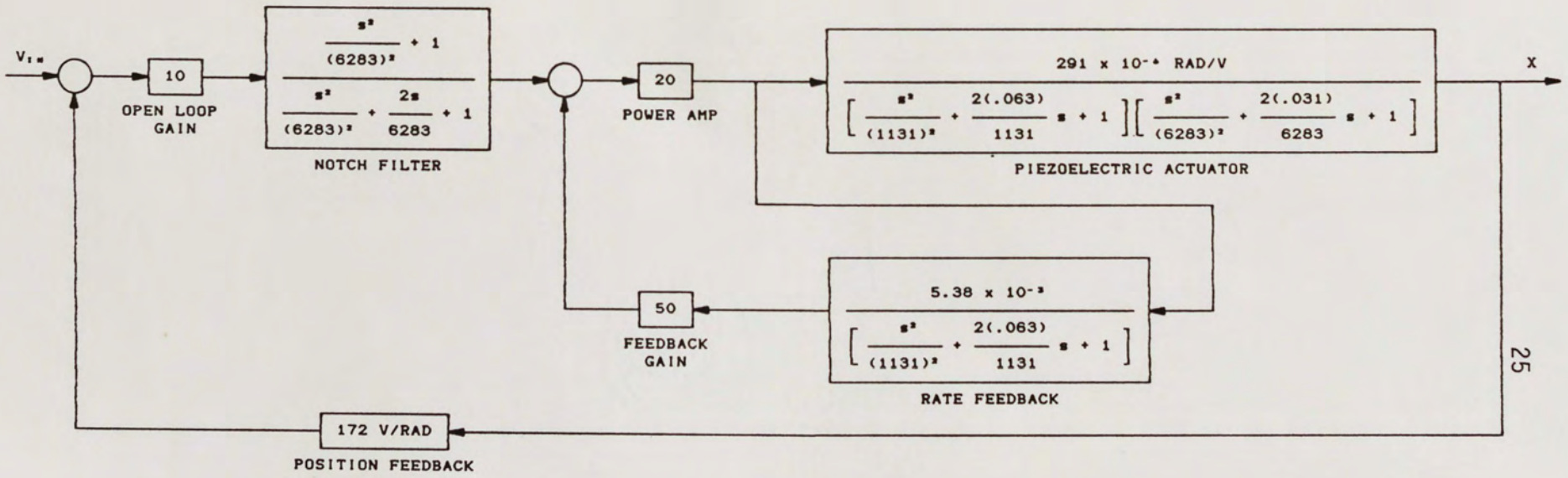

Figure 9. System Representation of Scanning Mirror System.

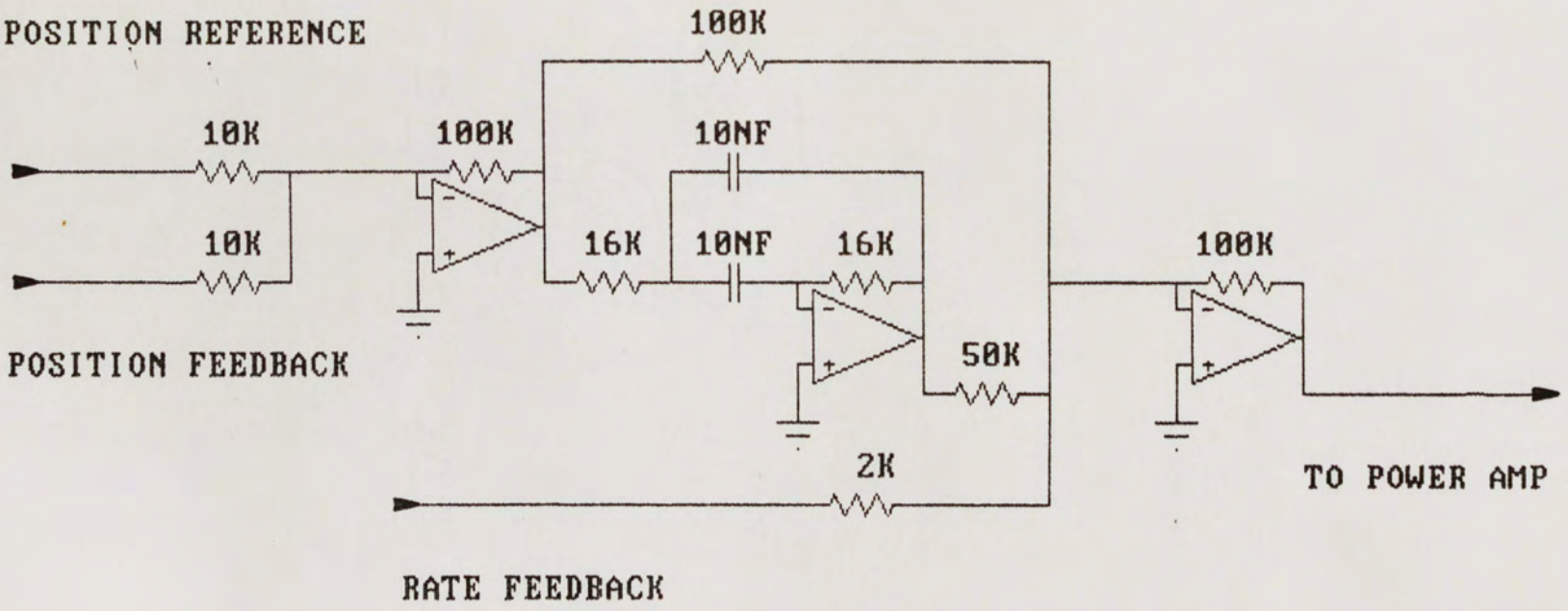

FIGURE 10. SCANNING MIRROR SYSTEM CONTROL.

position reference from a signal generator. These inputs are summed by the first op amp shown and the open loop gain, A_{OL} equal to ten, is inserted. The central portion of Figure 10 is a biquadratic notch filter that is tuned to the frequency 1000 hertz to attenuate the secondary resonance of the actuator. The notch filter implements the compensation transfer function $H_c(s)$. This is a unity gain path, except at the notch frequency, from the output of the summing op amp to the control output, labeled "to power amp." The rate feedback signal is added to the notch filter output by the op amp that generates the control output. The rate feedback signal is amplified by a factor of fifty, which is shown as β in Figure 8.

Figure 11 shows the circuitry that generates the rate, or velocity, feedback. This circuit senses the current that is driving the actuator by placing a differential amplifier across a 100 ohm resistor that is in series with the actuator. Since the actuator is an energy storage device, much like a capacitor, the charge on the actuator is proportional to its position. Velocity is the rate of change of position and current is the rate of change of charge. Thus the differential amplifier output, generated by detecting the voltage across the series current sense resistor, is proportional to the velocity of the actuator. The output of the differential amplifier is applied to a lowpass filter with complex poles that are the same as the complex poles of the actuator transfer function that create

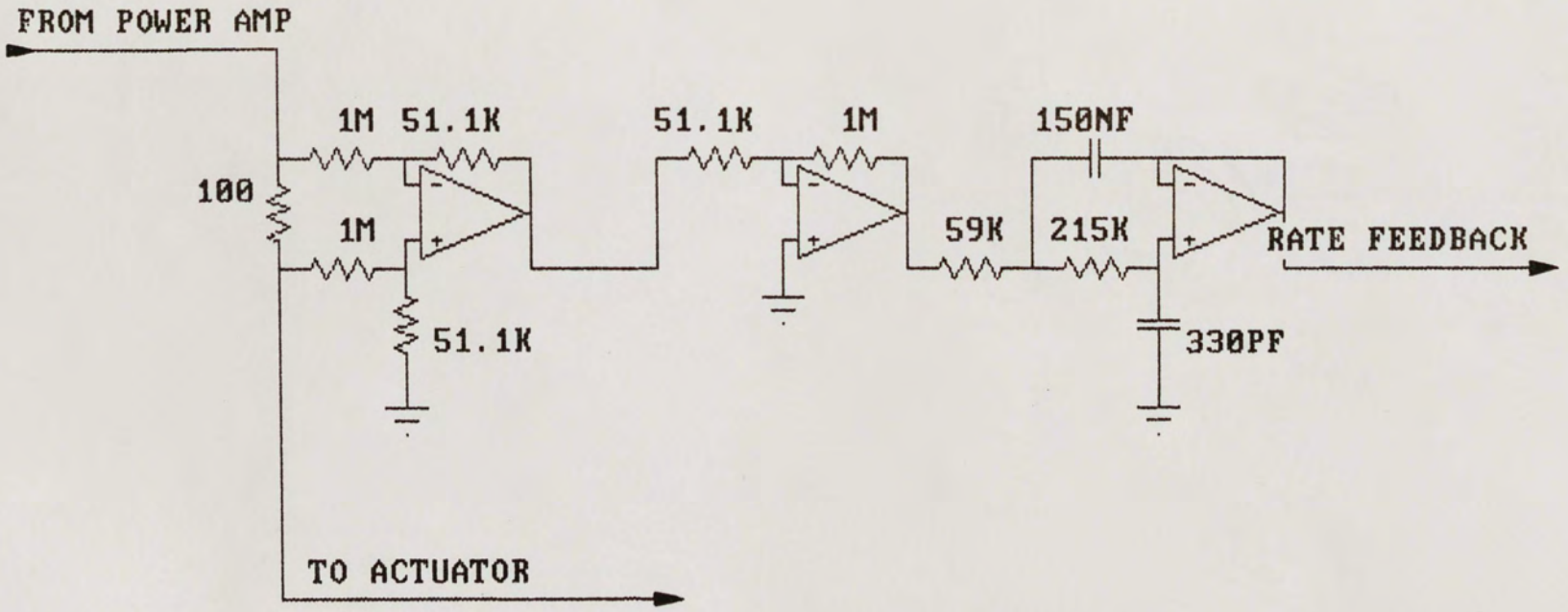

FIGURE 11. RATE FEEDBACK.

the primary resonance. By placing these poles in the feedback path of the scanning mirror system, the poles of the rate feedback become zeroes in the system transfer function and cancel the poles of the actuator transfer function associated with the primary resonance. This is how the rate feedback circuit attenuates the primary resonance of the actuator.

The position feedback is generated by introducing a local magnetic field into the vicinity of each of the two piezoelectric benders the make up the actuator. This field is created by an inductor, positioned very close to the bender on the side opposite the mirror, that is part of a FET Colpitts oscillator. The nickel electrodes that are on the outer surfaces of the bender are conductors that move in the field set up by the inductor. As the bender moves in the field, the impedance of the inductor changes. This change in impedance is manifested as a change in the magnitude of the oscillator output. The closer the bender is to the inductor, the lower the amplitude of the oscillations. Two oscillators, shown in Figure 12, are used so that an inductor is located behind each bender. The frequencies of the oscillators are set about 100 kilohertz apart to minimize generation of beat frequency signals. The amplitudes of the two signals generated by the oscillators are rectified and filtered. Finally, a differential amplifier is used to generate a signal proportional to the difference of the magnitudes of the outputs of the oscillators. The output of

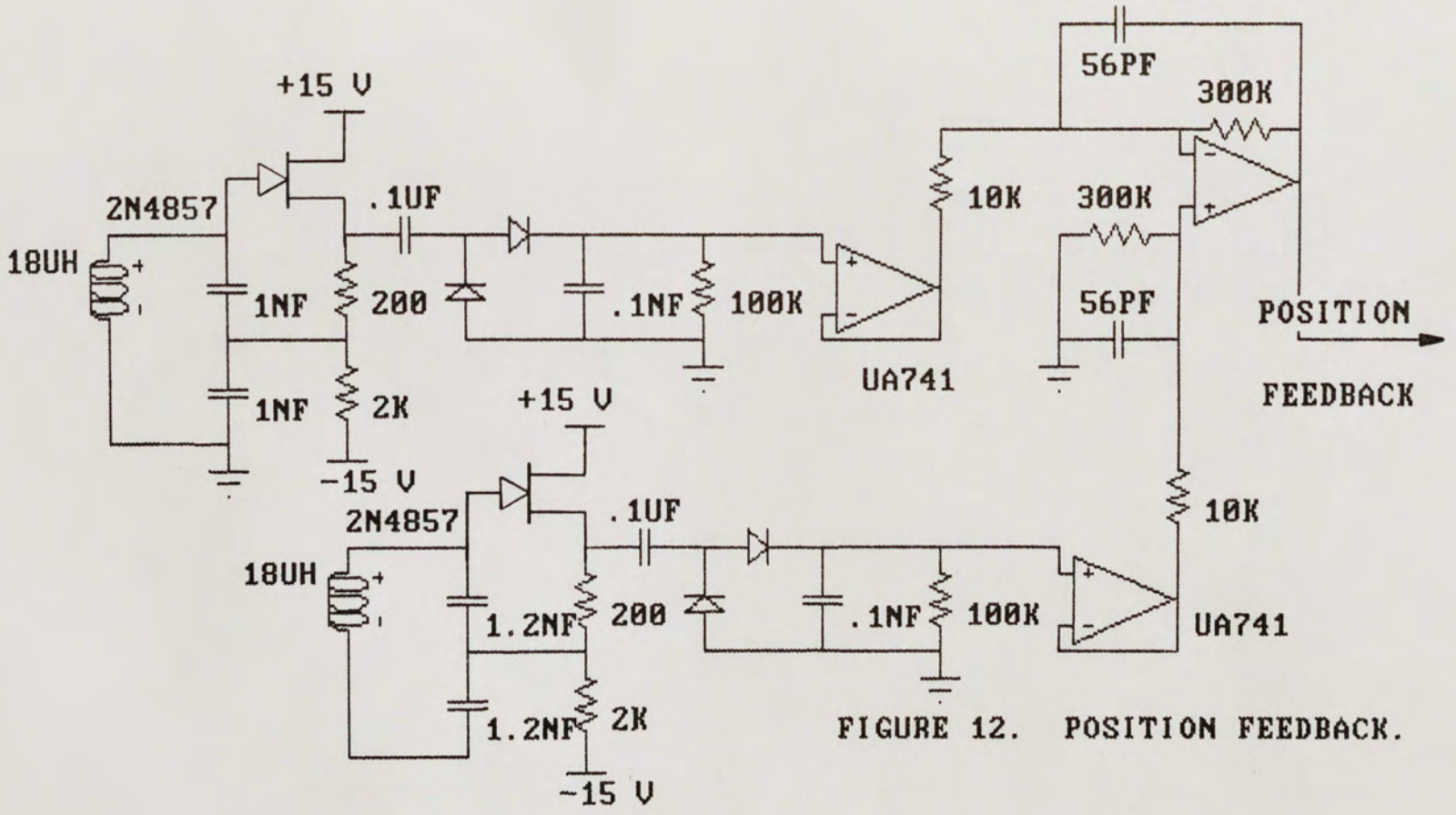

FIGURE 12. POSITION FEEDBACK.

the differential amplifier follows the position of the benders and is called the position feedback signal.[11]

The hysteresis that is characteristic of the piezo-electric bender is overcome using the position feedback. Hysteresis effects occur after a voltage has been applied to the bender to deflect it. Upon the removal of the voltage, the bender does not immediately return to its undeflected position. The dual-oscillator position detector senses this position difference due to hysteresis and introduces a voltage into the scanning mirror system to force the bender back to its undeflected system.

The output of the scanning mirror system control circuit in Figure 10 becomes the input of the power amplifier shown in Figure 13. The 100 ohm current sense resistor in series with the actuator and used by the rate feedback is shown again in this figure for clarity. The power amplifier uses a pair of high voltage PA08 op amps in a bridge configuration to double the peak-to-peak output voltage swing and provide voltages capable of producing significant actuator deflection. Since the PA08 operates from a ± 150 volt supply, the bridge configuration doubles the voltage swing applied to the actuator to ± 300 volts. Although the gain of the power amplifier is shown in Figure 9 as twenty, the gain of the circuit used by the original scanning mirror system, shown in Figure 13, is ten. The ten ohm resistors across pins one and two and across pins one and eight of each PA08 serve to prevent the current of the output stage of the op

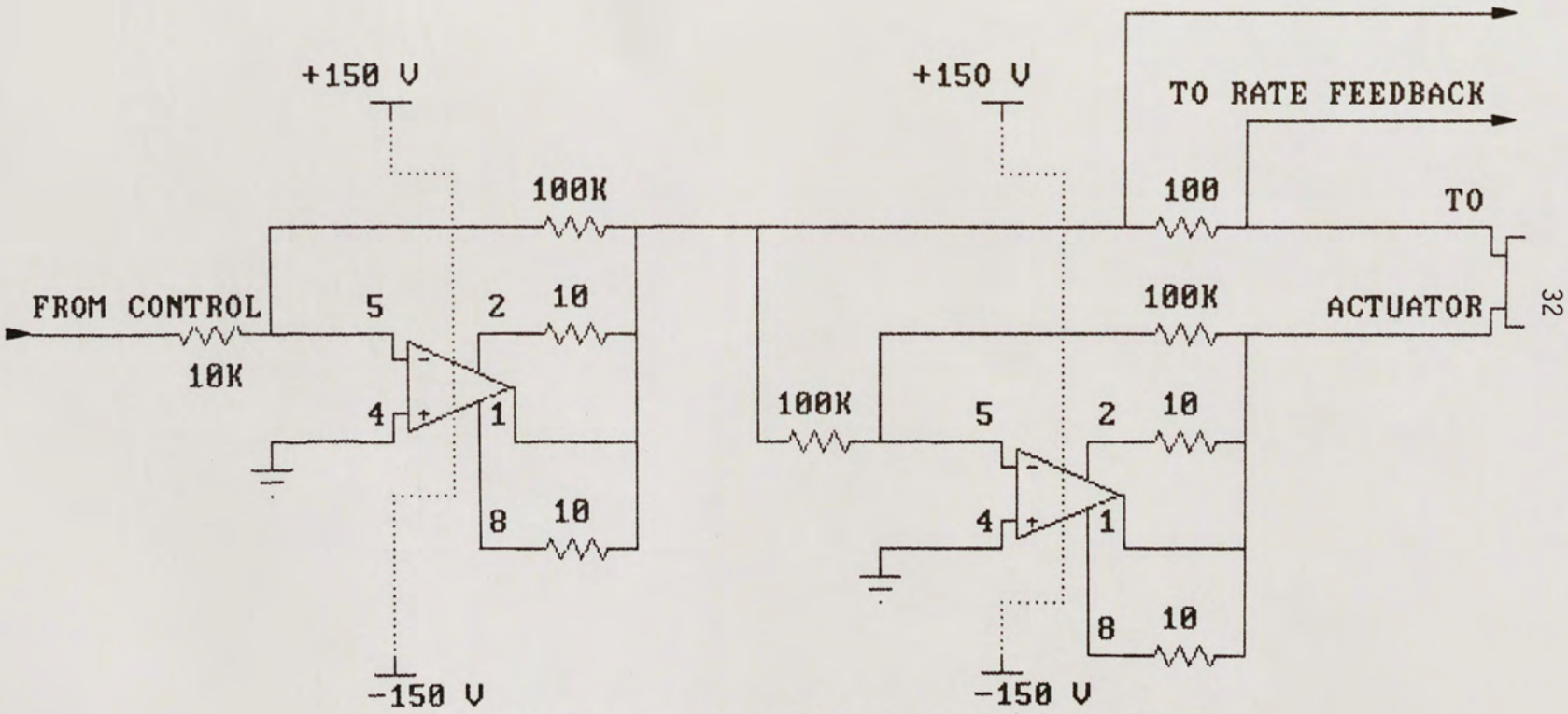

FIGURE 13. PA08 BRIDGE POWER AMPLIFIER.

amp from exceeding the current handling capability of the PA08 transistor geometry and wire bonds.[8] When configured with the current limit resistors as shown in Figure 13, the power amplifier is capable of driving capacitive loads up to 0.4 microfarads. For this reason, the power amplifier is particularly well-suited to drive the actuator since the actuator appears as a capacitive load to the power amplifier.[11]

The scanning mirror performance is shown by the frequency response plots in Figure 14 and Figure 15.[11] The legend on these figures refers to the measured values for the original scanning mirror system as the prototype and the plots that result from the MICRO-CAPII simulation analysis as the model. The open position loop response is shown in Figure 14, which shows that with a slight gain increase, the bandwidth is about 380 hertz with a phase margin of 30 degrees. The phase scale in Figure 14 and Figure 15 includes an additional phase inversion, so instability occurs when the phase reaches -360 degrees instead of -180 degrees. The closed position loop response is shown in Figure 15 and demonstrates the linear response of the system for the frequencies below the bandwidth frequency. The performance characteristics of the original scanning mirror system are listed in Table 1.

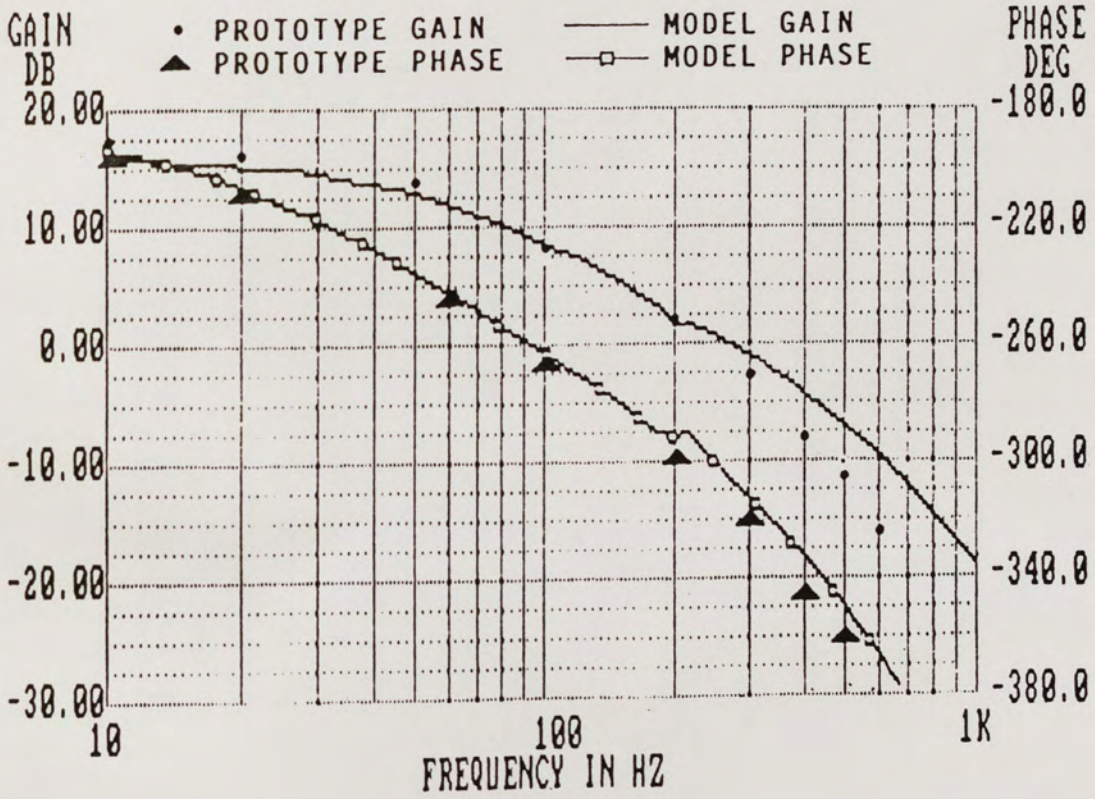

Figure 14. Open Position Loop Frequency Response.

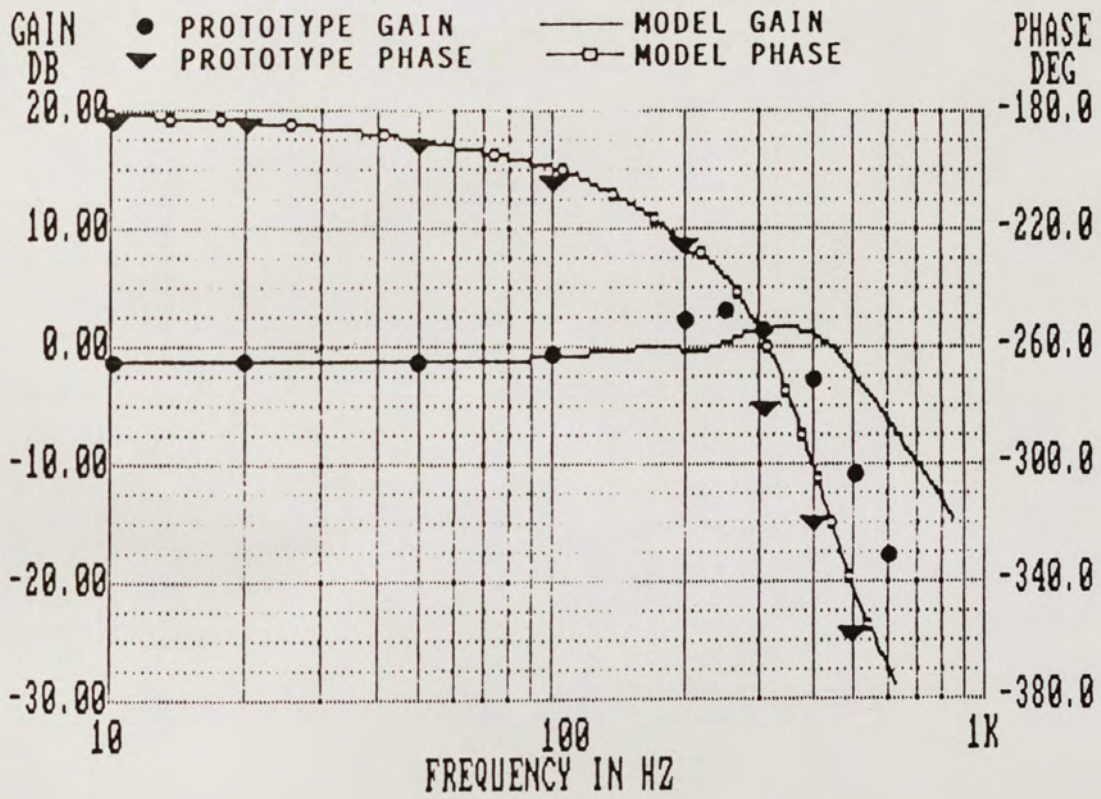

Figure 15. Closed Position Loop Frequency Response.

TABLE 1

SCANNING MIRROR SYSTEM PERFORMANCE

PARAMETER	VALUE
Static Position Loop Accuracy	9.09 %
Closed Loop Bandwidth	380 Hz
Gain Margin	10.4 dB
Phase Margin	30°
Maximum Deflection (300 volts p-p)	± 4.5°
Maximum Slew Rate	0.89°/sec

LIMITATIONS OF THE SCANNING MIRROR SYSTEM

The performance characteristics of the original scanning mirror system leave some room for improvement. The original system has a static position loop accuracy of 9.09 percent, which is a measure of the accuracy with which the output of the control system tracks a reference input. An accuracy of nearly 10 percent seems excessive and may be easily improved by modifying the control system. This parameter is effectively the steady-state error of this position control system and will be addressed in a later section.

The closed loop bandwidth of the original system is about 380 hertz. This figure is actually the small-signal bandwidth of the system because testing of the original scanning mirror system shows that the large-signal bandwidth is closer to 270 hertz. The large-signal bandwidth is referred to as the power bandwidth of the system.

The power bandwidth is measured by driving the system with an input whose magnitude produces the maximum angular deflection of the mirror. The maximum deflection that is obtained is closer to ± 3.0 degrees, which differs from the ± 4.5 degrees reported for the original system.[11] The deflection of ± 4.5 degrees may correspond to driving the actuator at the maximum power amplifier voltage swing of

300 volts peak to peak. During testing, the drive voltage swing could not exceed 180 volts peak to peak due to the limitations of the signal generator used to provide the reference input. At frequencies above 270 hertz, the system begins to distort, which is manifested by a displacement offset and loss of symmetry of the reflected light beam. These observations may be attributed to a combination of high steady-state error and the limited power bandwidth.

The bandwidth of the system is an indication of the time response of the system. A system with a large bandwidth has a faster rise time since higher-frequency signals are passed to the output.[4] If the scanning mirror system is modified to increase its power bandwidth, not only will the distortion effects described above be minimized, but the response time of the system will decrease, thereby enhancing system performance. This improvement, coupled with elimination of the nearly 10 percent position error, should serve to linearize the performance of the system over a broader range of frequencies. A subsequent section will describe a method of modifying the control system using a cascade of series compensators to increase the power bandwidth. Let us first examine possible reasons for the observed bandwidth limitation.

The power bandwidth may be limited by the slew rate of the power amplifiers shown in the schematic of the scanning mirror system in Figure 13. If the maximum slew rate that can be achieved by the system is less than the maximum slew

rate of the power amplifier, then the slew rate of the system is not limited by the selection of the op amps used in the power amplifier. However, there appears to be a discrepancy in the measured maximum slew rate of 0.89 degrees/second reported for the original system. Measurements of the system slew rate obtained using the original system show that the system slew rate varies from about 400 degrees/second at 10 hertz to a maximum value of nearly 20000 degrees/second for frequencies above 600 hertz. At the bandwidth frequency of 380 hertz for the original system, the slew rate is about 13 degrees/millisecond. If the reported slew rate were intended to be 0.89 degrees/millisecond, and the discrepancy arose due to a typographical error, the reported slew rate would have been measured at about 25 hertz.

The typical slew rate of the PA08 power op amps used in the actuator power amplifier is 30 volts/microsecond.[8] The measured maximum slew rate of the scanning mirror system is 20 degrees/millisecond, which can be converted to the same units for comparison. The maximum peak to peak voltage that may be applied to the actuator is 300 volts which produces a maximum mirror swing of ± 4.5 degrees. The slew rate of the scanning mirror system is

$$\frac{20000 \text{ degrees}}{\text{second}} \times \frac{300 \text{ volts}}{9 \text{ degrees}} = 0.66 \text{ volts/microsecond.}$$

The 0.66 volts/microsecond slew rate of the scanning mirror system is much less than the typical slew rate of

30 volts/microsecond for the power op amps. For this reason, the scanning mirror system slew rate does not seem to be limited by the slew rate of the power op amps.

The slew rate of the scanning mirror system may be limited due to the capacitance of the actuators that the power amplifier must drive. Slew-rate limiting for an op amp is caused by a capacitor associated with the op amp that charges at a fixed rate. The capacitor may be part of the internal op amp circuit or may be part of the external load applied to the op amp.[1] For the scanning mirror system, the limiting capacitance may be the capacitance of the piezoelectric actuator.

The rate at which the voltage changes with time across a capacitor C is given by

$$\frac{dv}{dt} = \frac{i}{C},$$

where i is the current through the capacitor. The current through the actuator is the output current of the PA08 op amps used in the power amplifier. The output current of the op amp is limited by the selection of the two current limiting resistors R_{CL} that are shown in Figure 13 across pins one and two and across pins one and eight of each PA08. The value for each R_{CL} is calculated according to

$$R_{CL} = 650 / I_{LIM},$$

where I_{LIM} is the desired maximum op amp output current in

milliamps.[8] The values of R_{CL} from Figure 13 are ten ohms. Using the equation above, the maximum output op amp output current i_{MAX} is limited to 65 milliamps.

Let us assume the actuator presents a purely capacitive load to the output of the power amplifier. If the current available to the actuator is limited to i_{MAX}, then the maximum rate at which the voltage across it can change is

$$\left.\frac{dv}{dt}\right|_{max} = \frac{i_{MAX}}{C} .$$

The electrical capacitance C_e of each actuator is 39.4 nanofarads, from the description of the piezoelectric bender model. The two actuators are connected in parallel across the output stage of the power amplifier, so the load presented to the power amplifier is twice C_e. Using the maximum op amp output current I_{LIM} of 65 milliamps, the maximum rate at which the voltage across the actuators can change is

$$\left.\frac{dv}{dt}\right|_{max} = \frac{i_{MAX}}{C} = \frac{I_{LIM}}{2 \times C_e} = \frac{65\ mA}{78.8\ nF} = 0.82\ V/\mu s.$$

The calculated slew-rate limit of 0.82 volts/microsecond due to the capacitance of the actuators is greater than the measured scanning mirror system slew rate of 0.66 volts/microsecond. The slew-rate limit due to the capacitance of the actuators does not seem to restrict the scanning mirror system slew rate.

The power bandwidth that results from a slew-rate limit of 0.82 volts/microsecond can be calculated. The angular slew rate, using the scale factor of 9 degrees deflection per 300 volt swing, is

$$\frac{0.82 \text{ volts}}{\text{microsecond}} \times \frac{9 \text{ degrees}}{300 \text{ volts}} = 24.6 \text{ degrees/ms} .$$

When the actuators are driven by a sinusoid of frequency w_o, the angular displacement of the mirror can be described by

$$\theta(t) = \theta \sin w_o t .$$

The angular velocity w(t) is the derivative of $\theta(t)$, which is

$$w(t) = \frac{d\theta(t)}{dt} = \theta w_o \cos w_o t .$$

The maximum angular velocity of the mirror determines the slew rate according to

$$w(t) \Big|_{max} = \theta w_o = \theta 2\pi f_{BW} = SR ,$$

where f_{BW} is the bandwidth and SR is the slew rate. This equation is solved for the bandwidth as

$$f_{BW} = \frac{SR}{2\pi \theta} = \frac{24.6 \text{ degrees/millisecond}}{2\pi \times 9 \text{ degrees}} = 437 \text{ Hz} .$$

The bandwidth at the slew-rate limit due to the capacitance of the actuators is 437 hertz. This bandwidth is greater

than the measured bandwidth of the scanning mirror system of 380 hertz. Again, the slew-rate limit due to the actuator load capacitance does not seem to restrict the system power bandwidth.

Since none of the factors considered seems to restrict the maximum slew rate, and hence the maximum power bandwidth, the original system design was examined while in operation. The source of the problem seems to be attributable to the rate feedback circuitry. At frequencies below 270 hertz, the signal produced by the rate feedback circuitry appears to be a relatively clean sinusoid. Above this frequency, the curves of the sinusoidal waveform, as observed on an oscilloscope, begin to become linear so that portions of the waveform begin to resemble a triangular waveform. At 460 hertz, the waveform barely resembles a sinusoid and is rife with slight discontinuities, or kinks, in the waveform. The conclusion is that the rate feedback saturates, beginning at about 270 hertz and that the slight distortion present at this frequency propagates through the feedback paths so that at higher frequencies the slight non-linearities are additive producing the dramatic distortion observed at 460 hertz. The simple solution to this problem is to replace the rate feedback with circuitry that still serves to attenuate the primary resonance of the bender model, while introducing minimal distortion or non-linearities that can be transmitted to the power amplifier and actuator.

NOTCH COMPENSATION FILTER DESIGN

The non-linearities observed in the rate feedback loop of the original mirror scanning system design seem to restrict the system bandwidth. The intent of the rate loop was to attenuate the primary resonance of the actuator. Since this portion of the system will be replaced, some method of providing this attenuation must be provided. The secondary resonance was attenuated with a biquadratic notch filter in the original design. An obvious alternative solution is to attenuate each of the actuator resonances with a separate notch filter. Two filters are cascaded to permit tuning each to properly attenuate the respective resonant peaks present in the magnitude response of the actuator model.

The use of biquadratic notch filters to attenuate the resonant peaks of the bender model is an example of pole-zero cancellation through the use of a bridged-T network as the the negative feedback of an active filter.[1] A pole-zero compensator realizes a transfer function that cancels the undesired complex-conjugate poles of the controlled process and introduces the poles of the compensator at more desirable locations in the s-plane.[4] The transfer function of the notch filter contains zeroes that cancel the complex-

conjugate poles of the bender model, which is the controlled process for this system, and poles that exhibit much smaller peak magnitudes at the resonant frequencies of the bender model. The use of a biquadratic filter effectively implements a compensator with two poles and two zeroes, as will be apparent shortly, in the transfer function of the notch filter.

The alternative solution alluded to above is used to attenuate the two resonant peaks that occur in the frequency response of the bender model shown in Figure 7. Two notch filters like that shown in Figure 16 are cascaded, so that the first filter will attenuate the first resonance while the second filter attenuates the second resonance. Each of the notch filters consists of a bandpass filter and a summing amplifier.

The bandpass filter transfer function $H_{BP}(s)$ is

$$H_{BP}(s) = \frac{-\dfrac{s}{R_2 C_2}}{s^2 + \left[\dfrac{1}{R_2 C_1} + \dfrac{1}{R_2 C_2}\right] + \dfrac{1}{R_1 R_2 C_1 C_2}} .$$

The quality factor of the bandpass filter is set to

$$Q_D = 0.5$$

by equating the values of the resistors and capacitors according to

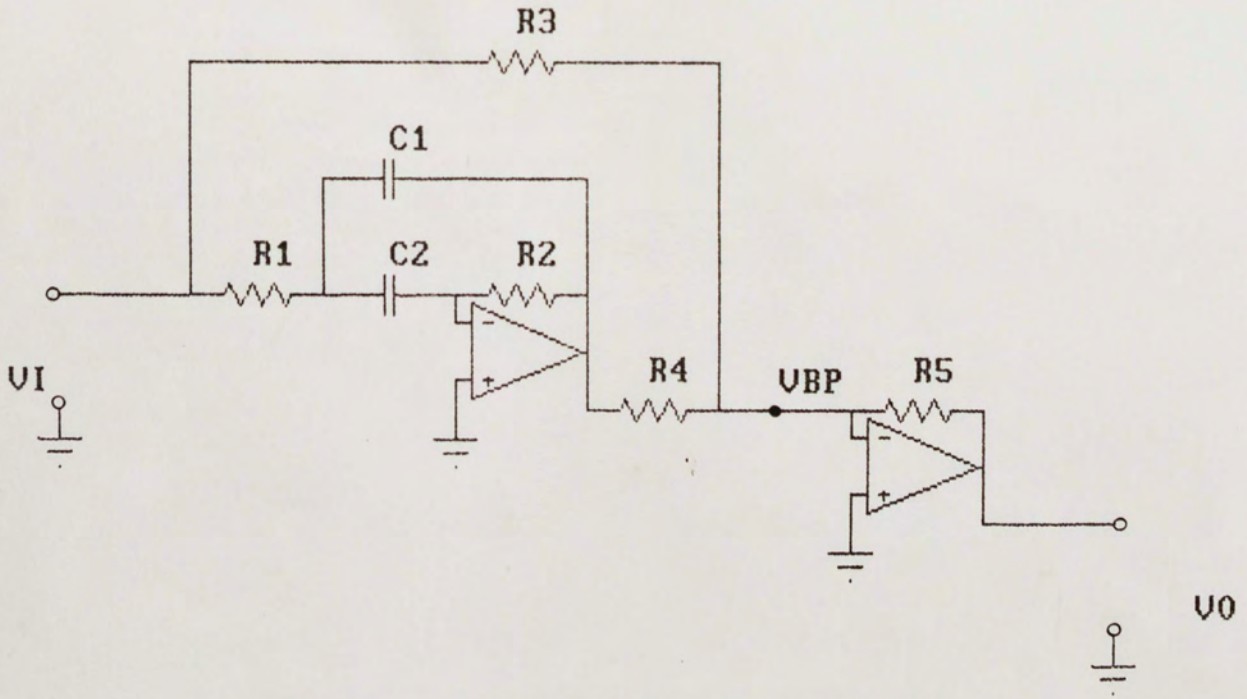

FIGURE 16. BIQUADRATIC NOTCH FILTER.

$$R_1 = R_2 \quad \text{and} \quad C_1 = C_2 .$$

This simplifies the bandpass filter transfer function to

$$H_{BP}(s) = \frac{V_{BP}}{V_I} = \frac{- w_D s}{s_2 + \frac{w_D}{Q_D} s + w_D^2} ,$$

where w_D is the pole frequency and Q_D is the pole quality factor.[1] The pole frequency is set by the values selected for R_1 and C_1 according to

$$w_D = \frac{1}{R_1 C_2} .$$

The transfer function $H_N(s)$ of the biquadratic notch filter is found by writing the equation for the sum of the voltages at the input of the summing amplifier as

$$V_O = - \frac{R_5}{R_3} V_I - \frac{R_5}{R_4} V_{BP} .$$

This equation is solved for V_O/V_I, which is equal to the desired transfer function $H_N(s)$ of the biquadratic notch filter. This transfer function is

$$H_N(s) = \frac{- \frac{R_5}{R_3} \left[\frac{s^2}{w_D^2} + \left[\frac{1}{Q_D} - \frac{R_3}{R_4} \right] \frac{s}{w_D} + 1 \right]}{\frac{s^2}{w_D^2} + \frac{s}{w_D Q_D} + 1} .$$

For each notch filter, w_D is set at one of the resonant frequencies of the actuator model. Component values are selected to make the numerator of each $H_N(s)$ for the two notch filters look exactly like each of the quadratics in the denominator of $H_A(s)$, the transfer function of the bender model. The two quadratics in the denominator $D_A(s)$ of $H_A(s)$ have the form

$$D_A(s) = \left[\frac{s^2}{w_A^2} + \frac{1}{Q_A} \frac{s}{w_A} + 1 \right] .$$

The expression for $D_A(s)$ is set equal to the numerator of $H_N(s)$ as

$$\left[\frac{s^2}{w_A^2} + \frac{1}{Q_A} \frac{s}{w_A} + 1 \right] = \left[\frac{s^2}{w_D^2} + \left[\frac{1}{Q_D} - \frac{R_3}{R_4} \right] \frac{s}{w_D} + 1 \right] .$$

This allows the zeroes in the numerator of the transfer function of the biquadratic notch filter to cancel poles in the denominator of the actuator transfer function when the two are cascaded. The values of the components of the notch filter are selected to set the pole frequency w_D of the notch filter equal to the resonant frequency w_A of the actuator. This permits the coefficients in the preceding expression to be equated as

$$\frac{1}{Q_A} = \left[\frac{1}{Q_D} - \frac{R_3}{R_4} \right] .$$

This expression is solved for R_3 to produce

$$R_3 = R_4 \left[\frac{1}{Q_D} - \frac{1}{Q_A} \right] .$$

The selection of the value of R_3 sets the attenuation at the pole frequency of the notch filter equal to the amount of the resonant peak of the actuator.

The pole frequency of first notch filter is set to 1131 radians/second, which is the primary resonant frequency of the actuator model. C_1 and C_2 are selected as 10 nanofarads, which sets the value of R_1 and R_2 at 88 kilohms. The value of R_4 is 50 kilohms and the value of R_5 is 100 kilohms. These two resistors are the same values used by the biquadratic notch filter used in the Tomasetti design. The value of R_3 is determined by the quality factor Q_A of the resonant peak of the primary resonance of the actuator model, the quality factor of the notch filter, and the value selected for R_4. For the actuator model described earlier, the value of Q_A for the first resonance is 7.16, which sets the value of R_3 at 93 kilohms.

The capacitors for the second notch filter are also selected as 10 nanofarads. The secondary resonance of the actuator model occurs at 6283 radians/second, which sets the values of R_1 and R_2 for the second notch filter at 16 kilohms. R_4 and R_5 are selected as 50 kilohms and 100 kilohms, respectively. The quality factor Q_A of the actuator model for the secondary resonance is 20, so the value of R_3 for the second notch filter is 97.5 kilohms.

The two cascaded biquadratic notch filters are shown in Figure 17 with the selected component values. The transfer function $H_{N1}(s)$ for the first notch filter is found by substituting the component values in the general form of $H_N(s)$ found above to produce

$$H_{N1}(s) = \frac{-2\left[\dfrac{s^2}{(1131)^2} + \dfrac{2(.070)}{1131}s + 1\right]}{\dfrac{s^2}{(1131)^2} + \dfrac{2s}{1131} + 1}.$$

In the same manner, the transfer function $H_{N2}(s)$ for the second notch filter is

$$H_{N2}(s) = \frac{-2\left[\dfrac{s^2}{(6283)^2} + \dfrac{2(.025)}{6283}s + 1\right]}{\dfrac{s^2}{(6283)^2} + \dfrac{2s}{6283} + 1}.$$

The two notch filters are cascaded with the actuator model to produce the open-loop magnitude and phase plot shown in Figure 18. The magnitude response shows the desired attenuation of the resonant peaks shown in the frequency response of the bender model of Figure 7. The magnitude of the resonant peaks M_P in Figure 7 at the resonant frequencies of 180 hertz and 1000 hertz are

$$M_{P1} = 7.94 \text{ (18 dB)}$$

and

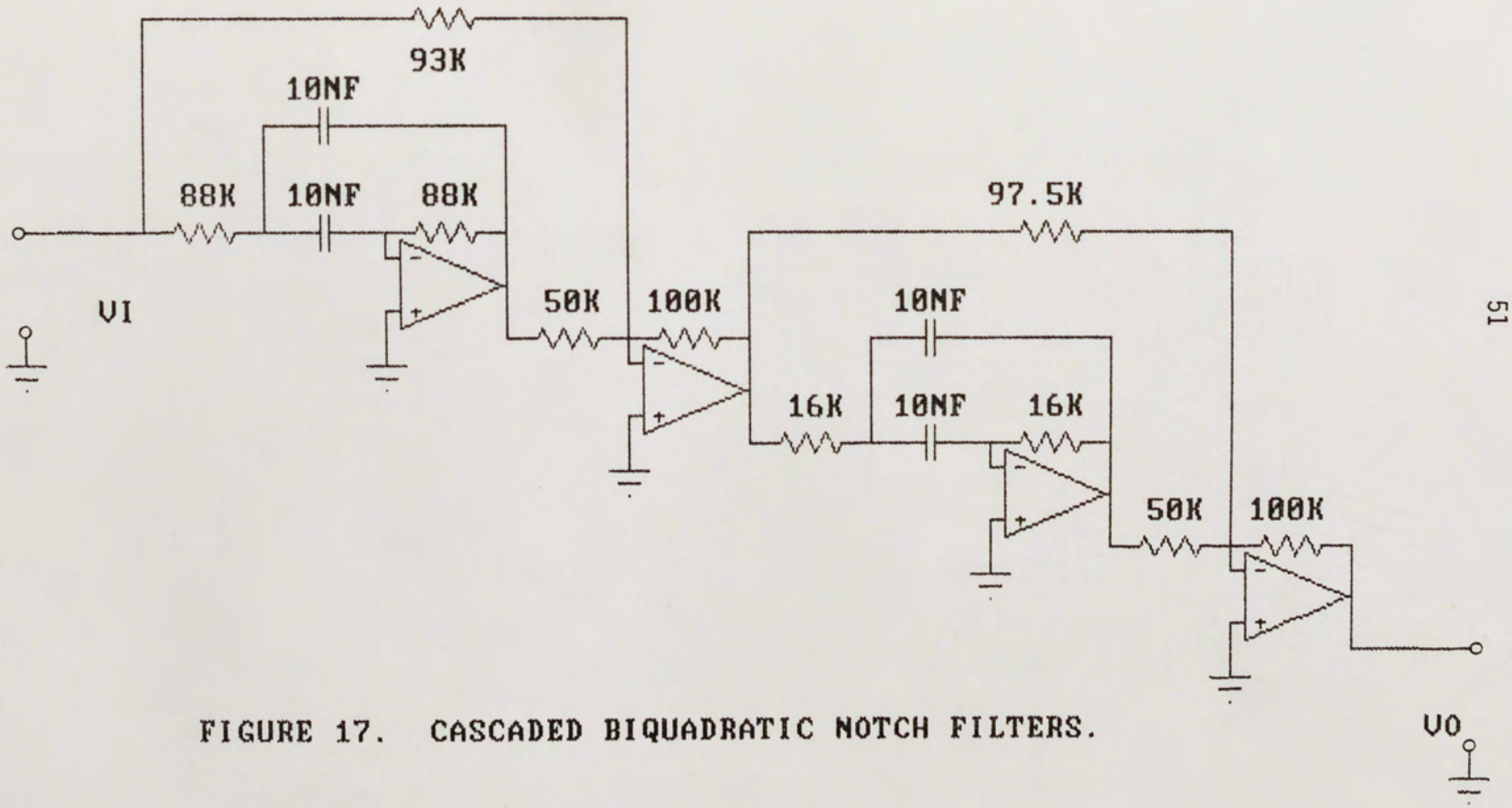

FIGURE 17. CASCADED BIQUADRATIC NOTCH FILTERS.

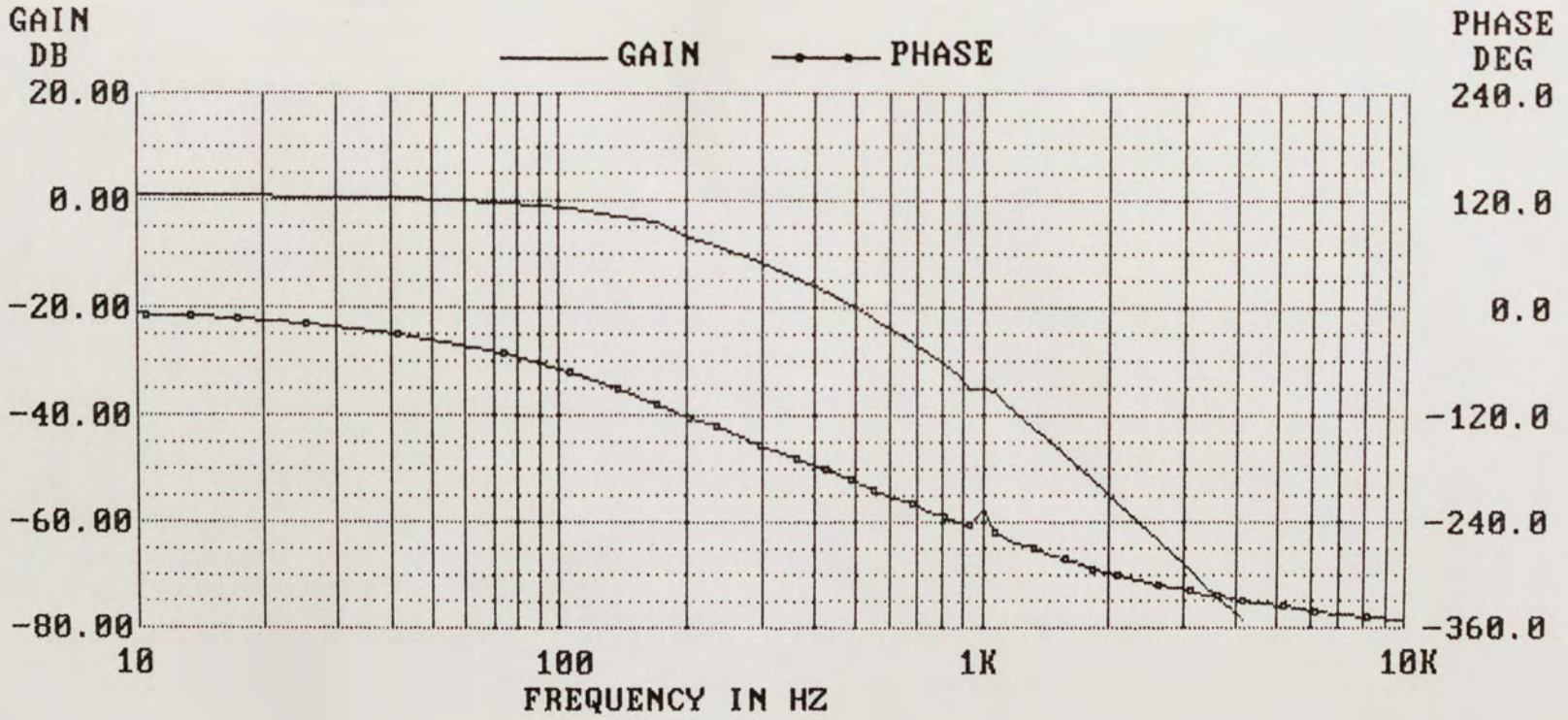

FIGURE 18. ATTENUATED RESONANT PEAKS FREQUENCY RESPONSE.

M_{P2} = 0.48 (-6.3 dB).

The response after the addition of the cascaded notch filters exhibits peak resonance values of

M_{P1}' = 1.77 (5.0 dB)

and

M_{P2}' = 0.018 (-35 dB).

The significant reduction in the values of the magnitudes of the resonant peaks achieved by the addition of the cascaded notch filters can be interpreted as a reduction in the peak overshoot in the step response of the system.[4]

The bandwidth of the bender model, whose frequency response is shown in Figure 7, is about 200 hertz while still maintaining a phase margin of 30 degrees. The response in Figure 18 exhibits a bandwidth of about 160 hertz with a phase margin of 90 degrees before any increase in gain. Adding gain equal to about 4 in the feed-forward path would increase the bandwidth to 300 hertz with a phase margin of 30 degrees. This performance approaches that of the original mirror scanning system. Although the relative stability of the system has been improved by an implied reduction in the peak overshoot, the objective, that of increasing the system bandwidth significantly, has yet to be achieved.

The performance exhibited by the frequency response of Figure 18 could be improved by the addition of leading phase

in the frequency range from 100 hertz to 1000 hertz, followed by an adjustment of the feed-forward gain. This indicates the need for additional series compensation in the form of a lead compensator, which will be described in detail in a following section.

SYSTEM COMPENSATION DESIGN CONSIDERATIONS

The original mirror scanning system exhibited a steady-state position error of 9.09 percent. One of the design objectives of this thesis is to improve this parameter. The steady-state error of a feedback control system is a measure of the difference between the actual output and the desired output signal. One of the main reasons for using feedback to produce a closed-loop control system is to reduce the steady-state error. The steady-state error of a stable closed-loop system is usually several orders of magnitude smaller than the error of the open-loop system.[2]

In control systems analysis, the steady-state response is defined as the fixed response of a system when time reaches infinity. Using this definition, a sinusoid is considered a steady-state response because its behavior is fixed for any time interval and when time reaches infinity. The steady-state response of a control system gives an indication of the final accuracy of the system. If the output response of a control system does not agree with the input exactly when time reaches infinity, the system is said to have a steady-state error.[4]

The steady-state error of feedback control systems depends on the input and the type of the system. When

determining the steady-state position error, the input of the control system is driven with a step function. The type of a control system is the number of integrators in the open-loop transfer function G(s).[4] For a type zero system with unity feedback, the steady-state error is dependent upon the closed-loop gain and the value of G(s) as s approaches zero in the limit. The constant K_p is defined as the steady-state position error and is equal to G(0).[2]

The steady-state position error for a system with nonunity feedback is found by analysis of the control system shown in Figure 19.

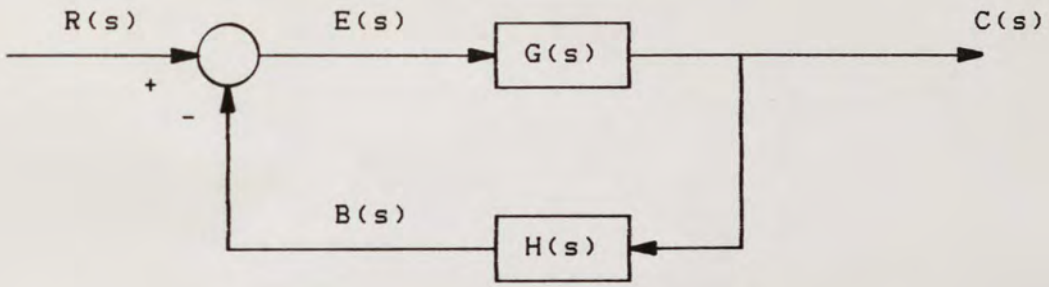

Figure 19. Nonunity Feedback Control System

In this figure, G(s) is the open-loop system transfer function and H(s) is the feedback transfer function. The reference input is R(s) and C(s) is the controlled output. The feedback signal is B(s) and the error signal is E(s). The error function E(s) of this control system is defined as

$$E(s) = R(s) - B(s) .$$

According to Figure 19, the Laplace transform of the error function is

$$E(s) = \frac{R(s)}{1 + G(s)H(s)} .$$

The final-value theorem is used to find the steady-state error e_{ss} as time approaches infinity and s approaches zero, which is

$$e_{ss} = \lim_{t \to \infty} e(t) = \lim_{s \to 0} sE(s) .$$

The expression for E(s) is substituted into this equation to produce

$$e_{ss} = \lim_{s \to 0} \frac{sR(s)}{1 + G(s)H(s)} ,$$

which shows that the steady-state error depends on the reference input R(s) and the loop transfer function G(s)H(s).[4]

For a step input R(s) of magnitude R, which has the Laplace transform R/s, the steady state error e_{ss} is

$$e_{ss} = \lim_{s \to 0} \frac{s(R/s)}{1 + G(s)H(s)} = \frac{R}{1 + \lim_{s \to 0} G(s)H(s)} .$$

The steady-state position error constant K_p is defined as

$$K_p = \lim_{s \to 0} G(s)H(s) .$$

With this definition, the steady state error for a nonunity

feedback control system is

$$e_{ss} = \frac{R}{1 + K_p} .$$

From this equation, the steady-state error is zero only when the error constant K_p is infinite. The steady-state error can be reduced to zero by the addition of a pole at zero, which is the same as the addition of one integration to the system open-loop transfer function G(s).[4] Such a system is referred to as a type 1 system.

If we return to the equation using the final-value theorem to find the steady-state error from above and replace G(s) with G(s)/s to show the addition of an integrator, then the steady-state error for a type 1 system is

$$e_{ss} = \lim_{s \to 0} \frac{s(R/s)}{1 + [G(s)/s]H(s)} = \frac{R}{1 + \infty} = 0 .$$

With this modification, the steady-state position error is reduced from the 9.09 percent accuracy that characterized the original system to zero for the modified system.

The question remains as to how to physically introduce an integrater in the system open-loop transfer function G(s). An integration compensation network added to the system will cause the steady-state position error to become zero. A phase lag compensator introduces a pole and a zero into the system open-loop transfer function. The pole and zero of the lag compensation network are placed at frequencies much lower

than the lowest frequency pole of the uncompensated system. The useful effect of the compensator is not the addition of phase lag, which can make the system unstable. Instead, it is the introduction of a pole that adds an integration to the transfer function to decrease the steady-state error that is the desired result.[2]

A phase lead compensation network is added to the system to add phase over a range of frequencies of interest. In this network, the pole and zero that are introduced are placed at frequencies on either side of the lowest frequency pole of the system transfer function. The maximum phase lead occurs halfway between these frequencies, so it is desirable to locate the pole and zero of the lead compensator so that the crossover frequency of the uncompensated system is halfway between the pole and zero frequencies of the lead compensator. The net effect of the addition of a lead compensator is the addition of leading phase to extend the bandwidth of the system by providing a satisfactory phase margin.[2]

LAG-LEAD COMPENSATION DESIGN

The foregoing discussion described the need for the addition of a series compensator to reduce the steady-state error, increase the bandwidth, and improve the phase margin of the frequency response of the series cascade of the two notch filters and the actuator model that is shown in Figure 18. A compensation network that has the desirable characteristics of both phase lag compensation and phase lead compensation is the lag-lead compensator shown in Figure 20. This compensator introduces an integrator in the form of a pole at the origin of the s-plane to reduce the steady-state error and introduces positive phase, or phase lead, to improve the phase margin and extend the bandwidth of the system.

The frequency domain transfer function T(s) of the lag-lead compensator is found using

$$T(s) = \frac{V_o}{V_i} = \frac{-Z_F}{Z_I} = \frac{-R_3 + \dfrac{1}{sC_2}}{R_1 \parallel \left[R_2 + \dfrac{1}{sC_1} \right]},$$

where Z_F is the feedback impedance and Z_I is the input impedance. The feedback impedance consists of the series

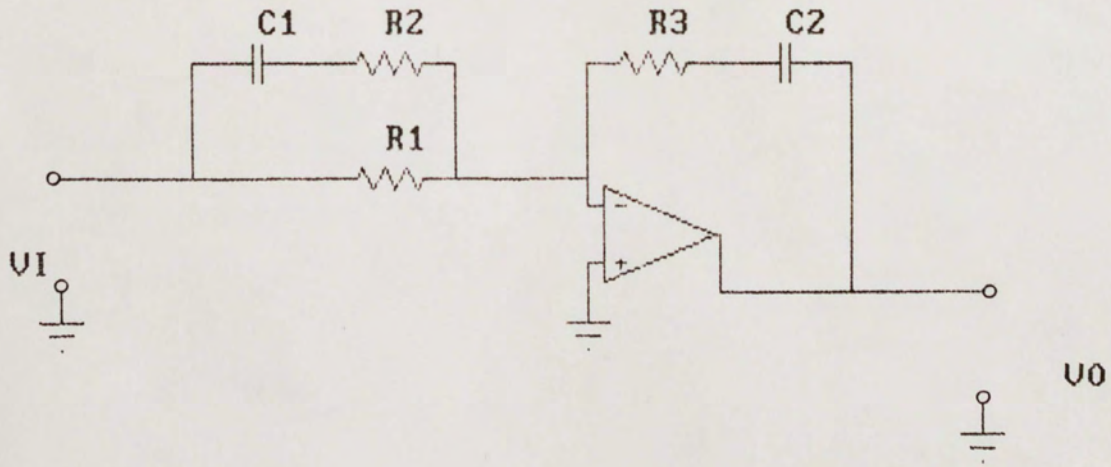

FIGURE 20. LAG-LEAD COMPENSATOR.

combination of R_3 and C_2 while the input impedance consists of the parallel combination of R_1 with the series combination of R_2 and C_1. When the above transfer function is simplified, the result is

$$T(s) = \frac{-(R_3C_2s + 1)[(R_1 + R_2)C_1s + 1]}{R_1C_2s(R_2C_1s + 1)}.$$

The numerator of the transfer function T(s) shows that this compensation network has two zeroes while the denominator indicates two poles, one of which is at zero frequency. The design of the compensation network is simplified by selecting the values

$$R_1 = R_3,\ C_1 = C_2,\ \text{and}\ R_1 >> R_2.$$

When these values are substituted into T(s), the compensator transfer function becomes

$$T(s) = \frac{-(R_1C_1s + 1)(R_1C_1s + 1)}{R_1C_1s(R_2C_1s + 1)}.$$

By noting that the frequencies at which the non-zero pole and the pair of zeroes occur are

$$w_P = \frac{1}{R_2C_1} \quad \text{and} \quad w_Z = \frac{1}{R_1C_1},$$

the transfer function T(s) is rewritten as

$$T(s) = -\frac{w_P}{w_Z}\,\frac{(s + w_Z)^2}{s(s + w_P)}.$$

This form of T(s) permits selection of the pole and zero frequencies to design the lag-lead compensator to provide the desired phase correction to extend the system bandwidth, provide the desired phase margin, and insure stability.

Analysis shows that the frequency f_z at which the zeroes should occur is 100 hertz, while the pole frequencies f_p occur at zero and 1000 hertz. The equations above for the pole and zero frequencies are used to calculate the component values for the circuit shown in Figure 20. The values for the capacitors C_1 and C_2 are selected as 10 nanofarads. The values for the resistors R_1 and R_2 are calculated using

$$R_1 = \frac{1}{2\pi f_z C_1} \quad \text{and} \quad R_2 = \frac{1}{2\pi f_p C_1} .$$

The circuit values for Figure 20 to produce a pair of zeroes at 100 hertz, a pole at zero, and a pole at 1000 hertz are

$$C_1 = C_2 = 10 \text{ nanofarads},$$

$$R_1 = R_3 = 16 \text{ kilohms},$$

and

$$R_2 = 160 \text{ kilohms}.$$

Using these component values, the transfer function T(s) becomes

$$T(s) = \frac{-628\left[\frac{s}{628} + 1\right]^2}{s\left[\frac{s}{6283} + 1\right]} .$$

When the values above are used in the lag-lead compensator of Figure 20, the magnitude and phase response produced is that shown in Figure 21. This plot ignores the phase inversion indicated by the negative sign in the numerator of T(s) so that the amount of phase lag and phase lead provided by the compensator can be read directly from the phase scale. Note that for frequencies below 100 hertz, the compensator introduces phase lag. Above 100 hertz, the compensator introduces phase lead. The amount of the phase lead increases from zero at 100 hertz to almost 45 degrees for frequencies between 300 and 800 hertz.

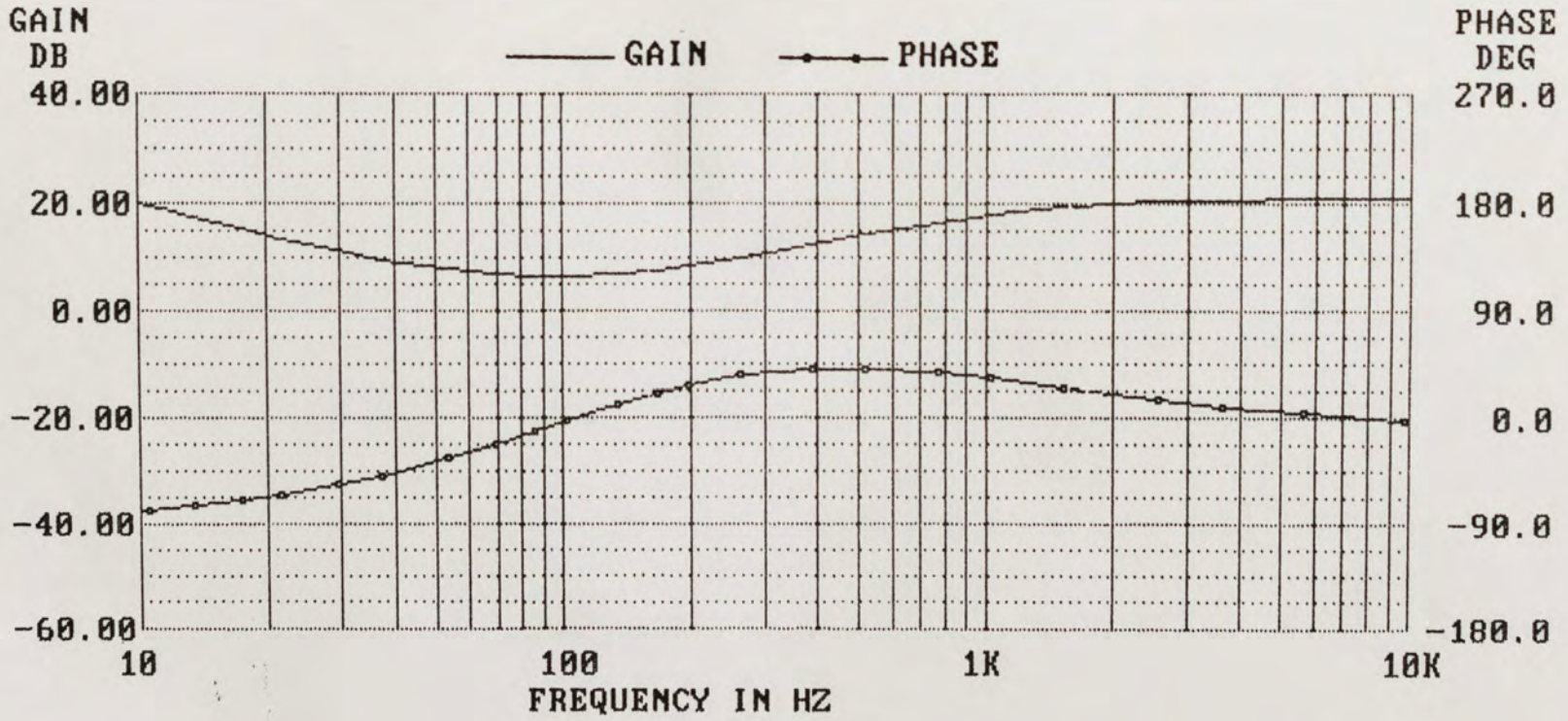

FIGURE 21. LAG-LEAD COMPENSATOR FREQUENCY RESPONSE.

AN IMPROVED SCANNING MIRROR SYSTEM

The system performance improvement can be seen by assembling the system components that have been described. The two biquadratic notch filters are cascaded with the lag-lead compensator and are tied to the power amplifier which, in turn, drives the piezoelectric bender model.

The open-loop frequency response that this assembly produces is shown in Figure 22. This response is compared with the response shown in Figure 18 to show the bandwidth improvement gained by the addition of the lag-lead compensator. The response in Figure 18 exhibits a bandwidth of about 160 hertz with a phase margin of 90 degrees before any increase in gain. Adding gain equal to about 4 in the feed-forward path would increase the bandwidth to 300 hertz with a phase margin of 30 degrees. The compensated response, in Figure 22, has a bandwidth of 300 hertz with a phase margin of 60 degrees. In Figure 18, instability occurs at 400 hertz. With the addition of the lag-lead compensator, instability occurs at 750 hertz in Figure 22.

The introduction of additional feed-forward gain of about 1.5 increases the compensated bandwidth to 500 hertz while still maintaining a phase margin of 30 degrees. These and other performance parameters of the modified scanning

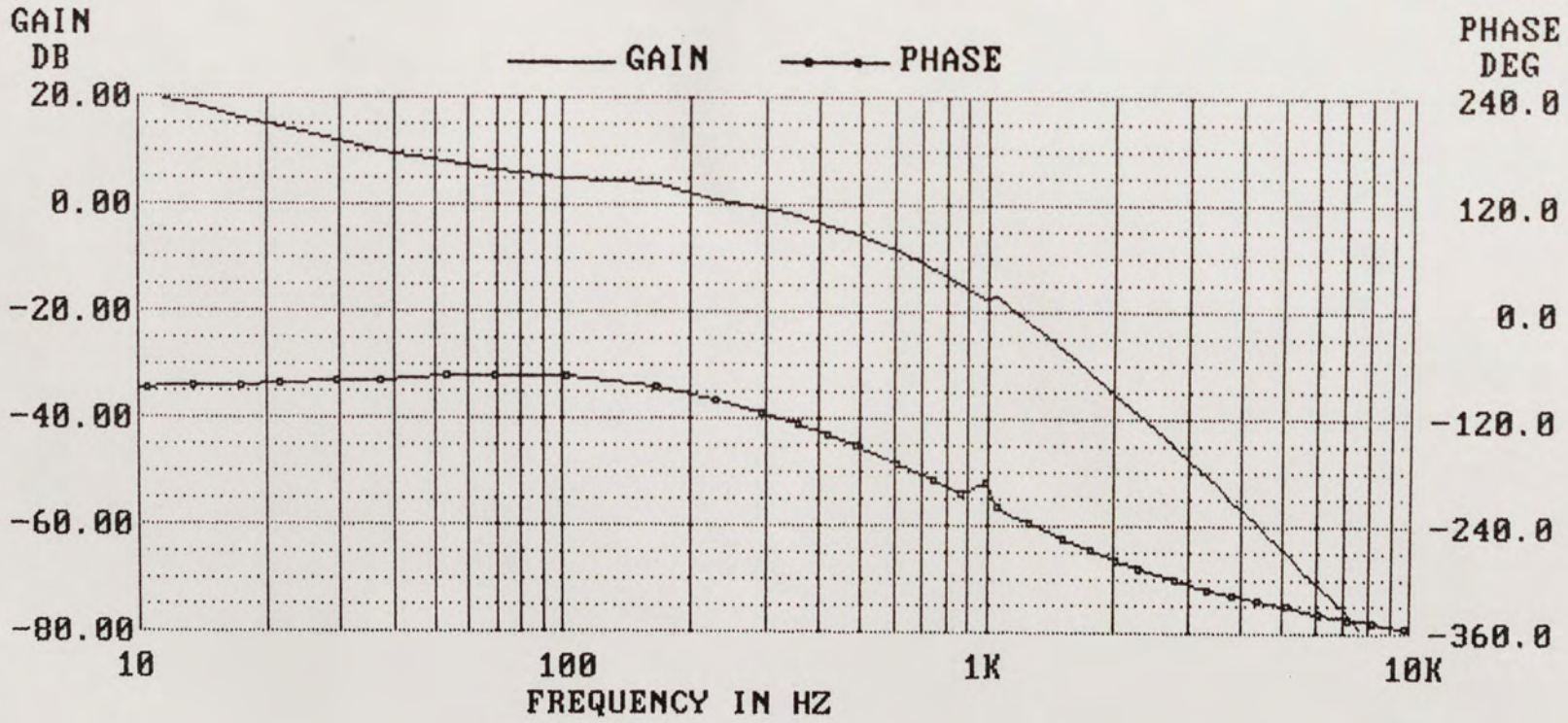

FIGURE 22. IMPROVED OPEN POSITION LOOP FREQUENCY RESPONSE.

mirror system with added feed-forward gain are listed in Table 2. These values can be compared to those in Table 1 for the original scanning mirror system to show the improvements in bandwidth and static position loop accuracy. The value for the maximum slew rate in Table 2 is also the correct value for the original scanning mirror system.

The improved scanning mirror system representation is assembled by collecting the transfer functions for the different system components. The transfer function $H_{N1}(s)$ for the first notch filter is

$$H_{N1}(s) = \frac{-2\left[\frac{s^2}{(1131)^2} + \frac{2(.070)}{1131}s + 1\right]}{\frac{s^2}{(1131)^2} + \frac{2s}{1131} + 1}$$

and the transfer function $H_{N2}(s)$ for the second notch filter is

$$H_{N2}(s) = \frac{-2\left[\frac{s^2}{(6283)^2} + \frac{2(.025)}{6283}s + 1\right]}{\frac{s^2}{(6283)^2} + \frac{2s}{6283} + 1}.$$

The lag-lead compensator was designed in the last section to produce the transfer function

TABLE 2

MODIFIED SCANNING MIRROR SYSTEM PERFORMANCE

PARAMETER	VALUE
Static Position Loop Accuracy	0
Bandwidth	380 Hz
Phase Margin	30°
Maximum Deflection (300 volts p-p)	± 4.5°
Maximum Slew Rate	20000°/sec

$$T(s) = \frac{-628\left[\frac{s}{628} + 1\right]^2}{s\left[\frac{s}{6283} + 1\right]} .$$

The transfer function for the power amplifier is simply a constant that is equal to a gain of ten that can be represented by A_{PA}. The transfer function of the actuator model that was presented earlier in this thesis is

$$H_A(s) = \frac{598 \times 10^{-6} \text{ radians/volt}}{\left[\frac{s^2}{(1131)^2} + \frac{2(.070)}{1131} s + 1\right]\left[\frac{s^2}{(6283)^2} + \frac{2(.025)}{6283} s + 1\right]} .$$

Combining all these transfer functions produces the open-loop system transfer function G(s), which is

$$G(s) = H_{N1}(s)\, H_{N2}(s)\, T(s)\, A_{PA}\, H_A(s) .$$

This equation becomes

$$G(s) = \frac{15}{\left[\frac{s^2}{(1131)^2} + \frac{2s}{1131} + 1\right]\left[\frac{s^2}{(6283)^2} + \frac{2s}{6283} + 1\right]} \times \frac{\left[\frac{s}{628} + 1\right]^2}{s\left[\frac{s}{6283} + 1\right]} \text{ radians/volt}$$

after substituting the transfer functions from above. The

position feedback that was a part of the original scanning mirror system is retained to minimize the hysteresis effects of the benders. The transfer function for the position feedback is the constant K_{PD}, which is equal to the value 172 volts/radian.[11] With the removal of the rate feedback circuitry, the feedback transfer function H(s) becomes K_{PD}.

The closed-loop transfer function M(s) has the form of a classical feedback control system, which is

$$M(s) = \frac{G(s)}{1 + G(s)H(s)} .$$

After the forms for G(s) and H(s) for the improved scanning mirror system are substituted, the expression for M(s) becomes

$$M(s) = \frac{15 \left[\frac{s}{628} + 1 \right]^2}{s \left[\frac{s}{6283} + 1 \right] D_{N1}(s)\, D_{N2}(s) + 2583 \left[\frac{s}{628} + 1 \right]^2} ,$$

where

$$D_{N1}(s) = \left[\frac{s^2}{(1131)^2} + \frac{2s}{1131} + 1 \right]$$

and

$$D_{N2}(s) = \left[\frac{s^2}{(6283)^2} + \frac{2s}{6283} + 1 \right] .$$

From the form of M(s), it becomes apparent the system does not lend itself well to paper calculations, which makes the MICRO-CAPII simulations more important for analyzing the system to determine its performance. When all the transfer functions are tied together, the block diagram that results is shown in Figure 23.

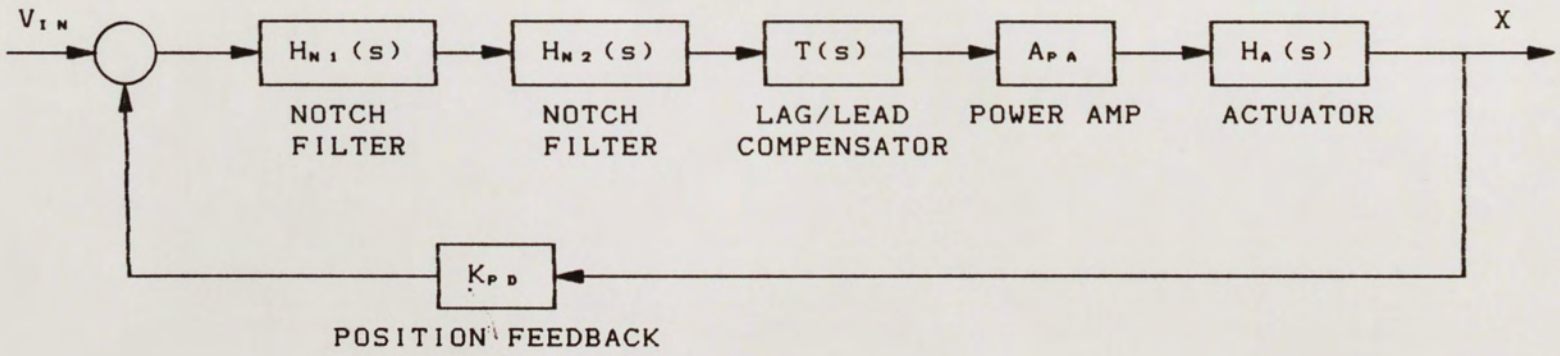

Figure 23. Improved Scanning Mirror System Block Diagram.

SUMMARY

This paper has presented a description of what ceramic piezoelectric devices are and how they can be used as an actuator in a scanning mirror system. An equivalent circuit model was developed to simulate the piezoelectric benders used by the system. A detailed description of such a system, designed and built by Thomas Tomasetti, was provided and its performance was enumerated. Limitations of the system were discussed and the reasons for the limits were explored. An alternative method of controlling the actuator was designed and analyzed as a proposed modification to the original Tomasetti design. These modifications entailed replacing the rate feedback with a pair of biquadratic notch filters and a lag-lead compensator. The resultant performance improvements were presented, based on analysis of the modified scanning mirror system.

Improvements were seen in the system power bandwidth and static position error. The original system demonstrated a bandwidth of 380 hertz and a static position error of 9.09 percent. With the proposed system modifications, the power bandwidth is extended to 500 hertz and the static position error becomes zero. A noteworthy point arises from the analysis that was done to find the source of the limitations

of the original system. The slew-rate limit was calculated based upon the capacitive loading of the actuators on the power amplifier. From the value for the slew-rate limit, the power bandwidth was calculated for this loading condition. It was found that the power bandwidth at the slew-rate limit is 437 hertz. What this means is that even with the system modifications installed, the piezoelectric bender actuator may not be capable of producing a power bandwidth of 500 hertz. The modified system also may have limitations that restrict its performance.

The most immediate area of further research can be found by reading this paper. These modifications have not been built, installed, or tested. There may be a whole assortment of wondrous surprises awaiting some unsuspecting graduate student. The research done to produce this paper has met its goal, however. The compensation approach to controlling a piezoelectric bender actuator does indeed appear to be one way to improve the original scanning mirror system performance.

REFERENCES

[1] Daryanani, Gobind. Principles of Active Network Synthesis and Design. New York: John Wiley and Sons, 1976, pp. 241-3, 301-302, 421-3.

[2] Dorf, Richard C. Modern Control Systems. Reading, Massachusets: Addison-Wesley Publishing Company, 1967, pp. 94-98, 302-310, 323-325.

[3] Germano, C. P. "Flexure Mode Piezoelectric Transducers," IEEE Transactions on Audio and Electroacoustics, Vol. 19, pp. 6-12, March 1971.

[4] Kuo, Benjamin C. Automatic Control Systems. 5th edition. Englewood Cliffs, New Jersey: Prentice-Hall Publishing Company, 1987, pp 296-300, 302-307, 502, 590.

[5] Martin, Robert J. Analysis and Synthesis of Active Feedback Applied to Piezoelectric Devices. Doctoral Dissertation. Orlando, Florida: University of Central Florida, 1984, pp. 6-8.

[6] MICRO-CAPII Electronic Circuit Analysis Program. Sunnyvale, California: Spectrum Software, 1986.

[7] "Modern Piezoelectric Ceramics." Bedford, Ohio: Vernitron Piezoelectric Division, p. 2.

[8] "PA08 Power Operational Amplifiers Data Sheet," Tucson, Arizona: Apex Microtechnology Corporation, 1985, pp. 1-4.

[9] "Piezoelectric Technology Data for Designers." Bedford, Ohio: Vernitron Piezoelectric Division, pp. 1-3, 12, 15-17.

[10] "Some Design Considerations in the Use of Bimorphs as Motor Transducers." Engineering Report. Bedford, Ohio: Vernitron Piezoelectric Division, p. 3.

[11] Tomasetti, Thomas J. Optimizing Scanning Mirror System Performance Using Solid State Piezoelectric Actuators. Master's Thesis. Orlando, Florida: University of Central Florida, 1986, pp. 3-9, 13-16, 35.

[12] Van Valkenburg, M. E. Analog Filter Design. New York: Holt, Rinehart, and Winston, 1982, pp 119-120.